Numerical Comparison of Mathematical and Computational Models for the Simulation of Stochastic Neutron Kinetics Problems

T.L. Gordon*, C.M. Cooling, M.M.R. Williams, M.D. Eaton

Nuclear Engineering Group, Department of Mechanical Engineering, City and Guild Building, Imperial College London, Exhibition Road, South Kensington Campus, London, SW7 2BX, United Kingdom

Abstract

This paper concerns numerical comparisons between five mathematical models capable of modelling the stochastic behaviour of neutrons in low extraneous (extrinsic or fixed) neutron source applications. These models include analog Monte-Carlo (AMC), forward probability balance equations (FPB), generating function form of the forward probability balance equations (FGF), generating function form of the backward probability balance equations (Pál-Bell), and an Itô calculus model using both an explicit and implicit Euler-Maruyama discretization scheme. Results such as the survival probability, extinction probability, neutron population mean and standard deviation, and neutron population cumulative distribution function have all been compared. The least computationally demanding mathematical model has been found to be the use of the Pál-Bell equations which on average take four orders of magnitude less time to compute than the other methods in this study. The accuracy of the AMC and FPB models have been found to be strongly linked to the computational efficiency of the models. The computational efficiency of the models decrease significantly as the maximum allowable neutron population is approached. The Itô calculus methods, utilising explicit and implicit Euler-Maruyama discretization schemes, have been found to be unsuitable for modelling very low neutron populations. However, improved results, using the Itô calculus methods, have been achieved for systems containing a greater number of neutrons.

Keywords: Pál-Bell, Itô Calculus, Survival Probability, Extinction Probability

1. Introduction

The deterministic neutron kinetics equations are the subject of many studies where the neutron population is large enough such that the fluctuations of individual neutron chains do not significantly contribute to the average behaviour of the system [1]. While very powerful when modelling large neutron populations, there exist applications where deterministic analyses are insufficient. Stochastic analyses are needed when the neutron population being modelled is low enough that individual neutron chains significantly impact the results; namely low neutron source sub-critical systems. A comprehensive review of stochastic neutron transport theory is provided by Pázsit and Pál [2]. There is a number of industrially important low neutron source problems such as nuclear waste assay, non-invasive or passive nuclear security interrogation for special nuclear materials (SNMs), and nuclear power plant start-up (NPP) analysis and also sub-critical experimental nuclear reactor physics measurements on nuclear reactor cores [3].

The accurate assay of small quantities of various fissile material samples are required for the safe operation of the nuclear fuel cycle [4]. Low-level process waste, leached fuel hulls, spent fuel rods, and separation columns are all examples in which spatial identification of their fissile material is required. As a consequence of the weak radiation signature of these small samples of radioactive materials it is important to utilise stochastic radiation transport methods for their assay.

Stochastic radiation transport methods can also be utilised in passive nuclear security interrogation [5, 6]. A 2014 report from the incident trafficking database, maintained by the International Atomic Energy Agency (IAEA), details a list of 2477 incidents involving the improper possession and movement of nuclear material and radioactive sources between the years 1993 and 2013 [7]. On this matter, two forms of nuclear security interrogation exist: active detection and passive detection, both of which aim to distinguish the nuclear signature of incoming materials from background radiation [7]. One form of active detection consists of inducing fission reactions with either fast neutrons or high energy photon sources and measuring the signature of the emitted radiation [8]. Passive detection simply consists of measuring the natural radiation emissions of the sample. While active detection produces a stronger radiation signal, and is easier to distinguish from background radiation, it is also more hazardous for the surrounding area. Passive detection is more favourable for safety reasons but is technically challenging. Passive detection needs to distinguish nuclear material from the radiation field of primordial isotopes U^{235}, U^{238}, and Th^{232} all of which emit alpha and gamma radiation either directly or through the decay of their daughter products. The

*Corresponding author
Email address: travis.gordon14@imperial.ac.uk (T.L. Gordon)

Received: 12 October 2020 / Accepted: 22 January 2021

background radiation is also contributed to by the spontaneous fission of U^{238}. Cosmic rays also contribute to this natural background radiation field. Fast protons in the upper atmosphere undergo a spallation type reaction with the atmosphere and generate fast neutrons. Once thermalized by elastic collisions with H^1, many cosmogenic radionuclides are produced, for example Be^7, which emits a gamma-ray signature. High fidelity stochastic radiation transport methods are required for this application such as the backward master equation (Pál-Bell equations) [6].

During nuclear power plant (NPP) start-up, the neutron population behaves stochastically and may deviate from the time averaged ensemble of the system [9]. Once the neutron population has risen substantially, the mean population becomes governed by deterministic neutron kinetic equations. Whether or not the neutron population is appropriately approximated by these equations depends on the nature (strong or weak) of the primary neutron start-up sources present [9]. The distinction between such sources has been discussed in depth by Hansen [9] who shows that a low extraneous neutron source, such that stochastic effects are prevalent, obey the Hansen criterion:

$$\Lambda S << \frac{\langle \nu(\nu-1)\rangle}{2\langle \nu\rangle} \approx 1 \tag{1}$$

where Λ is the neutron generation time, S is the source strength, and $\bar{\nu}$ is the mean number of neutrons produced per fission. Primary extraneous neutron start-up sources, such as Cf^{252} [10], are positioned in nuclear reactor cores to provide a reliable neutron detector count rate [11, 12]. If there is a low neutron flux, the count rate in the detector will be low and the control rods may be withdrawn to raise reactivity and thus the neutron flux. However, as the control rods are being withdrawn and reactivity further increased, the neutron flux may suddenly become very large and the doubling time very small [11, 12]. It is thus common practice to start-up a nuclear reactor in the presence of a sufficiently strong primary neutron start-up source such that the probability of the neutron population exceeding some predetermined fiducial level is appreciably small [11, 12]. However, due economic considerations, and for reducing the radiation dose to nuclear workers, through the handling of neutron sources, the ability to safely start-up a nuclear reactor without the use of such neutron sources has become the focus of various studies [11, 12, 13]. In the presence of a weak source, there exists a period of time during nuclear reactor start-up in which the neutron and delayed neutron precursor populations are low and modelling their statistical fluctuations is vitally important [14]. A significant amount of research work has been conducted on NPP start-up since the inception of nuclear power [15, 16, 17]. However, the focus of this study is the comparison in accuracy and computational efficiency of different mathematical methods capable of modelling the stochastic nature prevalent in general low neutron source systems. There is a wide variety of mathematical approaches to analysing low neutron source sub-critical and super-critical systems such as the analog Monte Carlo (AMC) method, forward probability balance equations (FPB), generating function form of the forward probability balance equations (FGF), generating function form of the backward probability balance equations (Pál-Bell), and Itô calculus. The aim of this paper is to assess the accuracy and computational efficiency of the various approaches using a variety of verification test cases. Currently there is no clearly agreed upon best approach to modelling such low neutron source systems. Therefore, the purpose of this study is, for the first time, to objectively compare such mathematical and computational models and provide numerical evidence for the accuracy and computational efficiency of the models in various low neutron source systems. In addition the validity and numerical limitations of using each mathematical and computational model will be discussed. Particular attention is focused on the Itô calculus approach and its numerical accuracy and computational efficiency for low neutron source sub-critical and super-critical systems.

The AMC method has been utilised in many studies for modelling low neutron populations in nuclear systems. In this method, individual neutrons and delayed neutron precursors are dealt with as discrete entities with each neutronic event simulated through the generation of a pseudo random number. Previous research work includes calculating the Probability of Initiation (PoI) [1, 18, 19]; size distribution of the neutron population along with the Probability of Extinction (PoE) in low neutron source systems [1, 18]; calculating k_{eff}, energy release, peak power [1]; and the probability distribution of the burst waiting time of neutron initiation [20]. The stochastic behaviour of low neutron population systems lends itself to such a mathematical modelling technique. However, as the neutron population increases, neutron kinetics and dynamics become more deterministic and the benefits of using the AMC method are reduced due to excessive computational requirements and the existence of computationally more efficient deterministic methods such as the point neutron kinetics approximation, whereby the AMC method is used during the stochastic regime and automatically switched to the point neutron kinetic approximation within the deterministic regime [1, 18].

Instead of modelling individual particle histories using the AMC method there also exists analytical approaches to stochastic neutron kinetics which are discussed by Hansen [9] and Bell [16, 17]. Particular attention was given to the probability distribution of obtaining different numbers of neutrons and the consequence of deviating from the deterministic approximation due to stochastic transients. This analytic approach, namely the FPB, requires the solution of an infinite set of ordinary differential equations (ODEs) to conserve the probability of the neutron population. This infinite set of ODEs may be reduced to a finite set of partial differential equations (PDEs) with the use of generating functions and will be referred to as FGF.

The Pál-Bell equations (PB) are a finite set of first order, coupled, non-linear ODEs [21, 22, 23]. Previous research work has investigated a wide variety of quantities of interest (QoI) using the Pal-Bell equations such as: the probability density function (PDF) of the neutron population, the moments of the PDF and

also the maturity time and source multiplier for low neutron source startup problems [5, 6, 11, 12, 13].

The final mathematical model to be compared in this study is an Itô calculus approach. Stochastic fluctuations can be introduced into the deterministic neutron kinetics equations by adding numerically generated noise into the terms of the equations. This allows the resultant equations to model stochastic phenomena [24]. Previously, Itô calculus approaches have been used to study a linear and discontinuous introduction of reactivity during nuclear reactor start-up [25], the random behaviour of neutron density and precursor concentration using explicit finite difference methods [26, 27], and implicit finite difference methods [28].

In this study we set out the relevant equations for each mathematical model and discuss the numerical comparisons made between the different approaches. The nuclear and neutron kinetics data used in this study is consistent between all models and is shown in Appendix A. Each distinct mathematical and computational model has been implemented within a modern fortran code and used to produce various numerical results and quantities of interest (QoI) depending on their capabilities. These numerical results and QoI are the following:

1. Survival Probability: The probability that there is at least one neutron in the system as a function of time. The initial condition is a starting neutron population of one and no external neutron source is present.
2. Extinction Probability: The probability that there are zero neutrons in the system as a function of time. The initial condition is a starting neutron population of zero and an external neutron source is present.
3. Neutron Population Mean: The mean neutron population as a function of time. The initial condition is a starting neutron population of zero and an external neutron source is present.
4. Neutron Population Standard Deviation: The standard deviation of the neutron population as a function of time. The initial condition is a starting neutron population of zero and an external neutron source is present.
5. Cumulative Distribution Function: The cumulative distribution function of the neutron population at a particular moment in time. The initial condition is a starting neutron population of zero and an external neutron source is present.

The survival probability, P_S, and extinction probability, P_E, are results that have been computed in many studies [13, 18, 29]. It should be noted that these probabilities are typically defined such that $P_S = 1 - P_E$. However, we have defined them slightly differently in this study in order to offer an extra method of comparison between the different models.

The ability of a mathematical model to simulate the stochastic behaviour of neutrons in practical low extraneous neutron source applications is greatly linked to its performance in computing the results detailed above. The survival and extinction probability offer a fundamental comparison of the models. However, particular attention will be given to the accuracy and computational efficiency of each model's ability to compute the mean, standard deviation, and cumulative distribution function. These three figures are fundamental for low source applications [1, 11, 12].

2. Mathematical Development

2.1. The Analog Monte-Carlo (AMC) Approach

In this model, a number of realisations are computed representing different potential system histories. In each, the number of prompt neutrons and the number of delayed neutron precursors in their respective groups are tracked as a function of time. Time is advanced in a number of small increments, with a probability of different neutronic events occurring in that interval. Each neutronic event then contributes in changing the populations at the next time step. The behaviour of the particular system being modelled can then be simulated from performing many realisations and the analysis of the population history of this ensemble of realisations generates extra statistical results.

The implementation of the AMC model closely follows the research work of Cooling et al. [1]. However, a simplification is made to the possible interactions of the neutrons within the system being analysed. The systems under study are assumed to be infinite in extent, and as such neutron capture and fission are the only two interactions considered, with the probability of a neutron escaping the system equal to zero. The total macroscopic neutron cross-section is given by:

$$\Sigma_t = \Sigma_a + \Sigma_s \tag{2}$$

$$\Sigma_a = \Sigma_c + \Sigma_f \tag{3}$$

where Σ_a is the macroscopic absorption cross-section, Σ_c is the macroscopic capture cross-section, Σ_f is the macroscopic fission cross-section, and Σ_s is the macroscopic scattering cross-section. The manipulation of these cross-sections facilitate changes in reactivity.

The probability of a neutron interaction with the atomic nuclei of the host medium is given by:

$$p_c = \frac{\sum_c}{\sum_t} \tag{4}$$

$$p_f = \frac{\sum_f}{\sum_t} \tag{5}$$

where p_c is the probability a neutron is captured by a non-fission process and p_f is the probability that a neutron causes fission.

Table 1: The probabilities of each possible neutron event and the effect each has on the system during the time dt.

Event	Probability	Effect on population	
		Prompt	Group m
Source emission	$S\,dt$	$+1$	/
Fission producing ν prompt neutrons	$p'_f p_\nu(1-\overline{\nu}\beta)$	$+\nu-1$	/
Fission producing ν prompt neutrons and one delayed precursor of group m	$p'_f p_\nu \overline{\nu}\beta_m$	$+\nu-1$	$+1$
Precursor decay of group m	$\lambda_m dt$	$+1$	-1
Neutron capture	$\frac{p_c}{\Lambda}dt$	-1	/
No event	$1-\frac{p_c+p_f}{\Lambda}dt$	/	/

The probability that these interactions occur during a small time interval dt is then:

$$p'_c = \frac{p_c}{l}dt \tag{6}$$

$$p'_f = \frac{p_f}{l}dt \tag{7}$$

$$p'_{surv} = 1 - \frac{p_c + p_f}{l}dt \tag{8}$$

where p'_c, p'_f, and p'_{surv} are the probabilities of capture, fission, and no event within small time interval dt respectively, and l is the mean neutron life time:

$$l = \frac{1}{v\sum_{\mathrm{a}}} \tag{9}$$

where v is the neutron speed.

For analyses that consider the effect of delayed neutron precursors, β_{m} is the fraction of neutrons produced by fission via the delayed neutron precursors belonging to group m, where $\beta = \sum_m \beta_m$ and $\beta \ll 1$. The average number of a delayed neutron precursor from group m being produced given a fission event is $\overline{\nu}\beta_m$ where $\overline{\nu}$ is the average number of neutrons produced in a fission event.

For each neutron in the system a pseudo random number is generated, from a uniform distribution, between zero and one, which determines if the neutron either survives the time-step, causes fission, or is captured. If a fission event does occur, the number of prompt neutrons emitted is ν with a probability p_ν. is The same process is performed for each neutron source with a random number determining whether the source releases a neutron into the system. A random number is also generated for each delayed neutron precursor to determine whether it decays adding a neutron to the state of the system at time $t + dt$ or survives the time-step and adds a precursor to the state at time $t+dt$. These fission events are summarised in Table 1.

Once the interactions of all prompt neutrons, delayed neutron precursors, and sources have been simulated, the process is repeated at the new time-step. Following the research work of Cooling et al. [1], the increment in time, dt, is chosen such that the probability of a single neutron interacting in multiple events, p'_{multi}, is sufficiently small (set at 10^{-4}). The value of dt varies with the state of the system via the following criteria. Firstly, if the system contains prompt neutrons at time t:

$$p'_{multi} \geq (1 - p'_{surv})^2. \tag{10}$$

If delayed neutron precursors are present in the system:

$$p'_{multi} \geq (p'_{decay,m})^2 \tag{11}$$

where $p'_{decay,m} = \lambda_m dt$ is the probability that a delayed neutron precursor of group m emits a neutron. If a neutron source is present in the system:

$$p'_{multi} \geq (p'_s)^2 \tag{12}$$

where $p'_s = S\,dt$ is the probability that the neutron source with strength $S\,(n/s)$ emits a neutron. The time-step dt is chosen such that it is the largest possible while adhering to all three criteria. The different results are readily extracted from the AMC model as it simulates discrete entities.

The implementation described above results in a reduction in the computing power required for the simulations. However, setting a value of p'_{multi} is an approximation and it is possible to avoid this discretization approximation. A pseudo random number can be generated to determine the life-time of each particle in the system as shown by Sutton [18] and Gang [20] which avoids the use of the approximation above. However, the AMC model described in this study is simpler to implement and is capable of producing very accurate results.

2.2. The Forward Probability Balance Equation

Bell [16] formulated an expression for the probability distribution function of the neutron population by accounting for all possible neutron events that can occur in the domain. Bell's expression facilitated multiple neutron sources. Here we replicate Bell's expression while only considering one neutron source and with a common notation that is used throughout this study:

$$\begin{aligned} P(n,\vec{c},t+dt) = &\left(1 - \frac{n dt}{l} - \sum_{m=1}^{M}\frac{c_m}{\tau_m}dt - S\,dt\right)P(n,\vec{c},t) \\ &+ \sum_{\nu=0}^{\nu_{\max}}(n-\nu+1)\frac{p_{\nu,0}(t)dt}{l}P(n-\nu+1,\vec{c},t) \\ &+ \sum_{\nu=0}^{\nu_{\max}}\sum_{m=1}^{M}(n-\nu+1)\frac{p_{\nu,m}(t)dt}{l}P(n-\nu+1,\vec{c}-\vec{\delta}_m,t) \\ &+ \sum_{m=1}^{M}\frac{c_m+1}{\tau_m}dtP(n-1,\vec{c}+\vec{\delta}_m,t) \\ &+ S\,dtP(n-1,\vec{c},t) \end{aligned} \tag{13}$$

where $P(n,\vec{c},t)$ is the probability that there are n prompt neutrons and $\vec{c}$ delayed neutron precursors in the system at time t, ν is the number of neutrons produced per fission, $p_{\nu,m}$ is the probability of ν prompt neutrons and a delayed neutron precursor of group m being produced, and $\tau_m = 1/\lambda_m$ is the inverse of the decay constant of precursor group m. (Eq.13) states that the probability of having n neutrons and c precursors at time $t + dt$ is equal to the summation of the following terms:

1. No event - The probability that no neutron events occur multiplied by the probability that there are n neutrons and $\vec{c}$ precursors at time t;
2. Fission without precursor - The sum over ν of the probability that a fission event occurs producing ν prompt neutrons and zero delayed precursors multiplied by the probability that there are $n-\nu+1$ neutrons and $\vec{c}$ precursors at time t;
3. Fission with precursor - The sum over ν and m of the probability that a fission event occurs producing ν prompt neutrons and one delayed precursor of group m multiplied by the probability that there are $n-\nu+1$ neutrons and $\vec{c}-\vec{\delta_m}$ delayed precursors of group m at time t;
4. Precursor decay - The sum over m of the probability that the decay of a precursor group m occurs multiplied by the probability that there are $n-1$ prompt neutrons and $\vec{c}+\vec{\delta_m}$ delayed precursors of group m at time t;
5. Source emission - The probability that a neutron source decays multiplied by the probability that there are $n-1$ neutrons in the system at time t.

By subtracting $P(n,\vec{c},t)$ from both sides and dividing by dt, the ODE can be formed [16]:

$$\begin{aligned}\frac{dP(n,\vec{c},t)}{dt} &= -\left(\frac{n}{l}\right)P(n,\vec{c},t) + \sum_{\nu=0}^{\nu_{\max}}(n-\nu+1)\frac{p_{\nu,0}(t)}{l}P(n-\nu+1,\vec{c},t)\\ &+ \sum_{\nu=0}^{\nu_{\max}}\sum_{m=1}^{M}(n-\nu+1)\frac{p_{\nu,m}(t)}{l}P(n-\nu+1,\vec{c}-\vec{\delta}_m,t)\\ &+ \sum_{m=1}^{M}\left[\left(\frac{c_m+1}{\tau_m}\right)P(n-1,\vec{c}+\vec{\delta}_m,t) - \left(\frac{c_m}{\tau_m}\right)P(n,\vec{c},t)\right]\\ &+ S(t)\Big(P(n-1,\vec{c},t) - P(n,\vec{c},t)\Big).\end{aligned} \tag{14}$$

As the method calculates the probability of distinct numbers of neutrons, the simulation can only model the probability of there being a number of neutrons and precursors in a finite range:

$$\begin{aligned} n &= (0,1,2,...,n_{\max})\\ c_m &= (0,1,2,...,c_{m,\max}) \qquad \text{for } m = 1,2,3,...,M.\end{aligned}$$

(Eq.14) computes the time differential of the probability that there are $(n,\vec{c})$ neutrons at time t. The implementation of this model requires the initial populations of the prompt neutrons and delayed neutron precursors to be in the form of a probability distribution. From these initial conditions, it is then possible to populate the above terms and calculate the gradient function for all $(n,\vec{c})$ combinations in the domain. With the calculated gradient functions, the probabilities that there are n neutrons and $\vec{c}$ precursors at the subsequent time-step $t+dt$ is calculated, and the cycle is repeated across the time domain $t = (0, t_{\text{end}})$. It is then straight forward to extract the required results.

It is important to note that this method requires approximations for calculating the probability that there are $n_{\max}$ prompt neutrons or $c_{m,\max}$ delayed neutron precursors in the system at any particular moment in time. This is due to the fact that the probability $P(n,\vec{c},t+dt)$ of having n prompt neutrons and $\vec{c}$ delayed precursors in the system at time $t+dt$, is a function of the probability $P(n+1,\vec{c},t)$ and $P(n,\vec{c}+\vec{\delta}_m,t)$. A similar relationship is also true for the delayed neutron precursors. As such, (Eq. 14) was modified to account for a maximum permissible neutron and precursor population:

$$\begin{aligned}\frac{dP(n,\vec{c},t)}{dt} &= -\left(\frac{n}{l}\right)P(n,\vec{c},t)\\ &+ \sum_{\nu=0}^{\nu_{\max}}(n-\nu+1)\frac{p_{\nu,0}(t)}{l}P(n-\nu+1,\vec{c},t)(1-\delta_{n,n_{\max}}\delta_{\nu,0})\\ &+ \sum_{\nu=0}^{\nu_{\max}}\sum_{m=1}^{M}(n-\nu+1)\frac{p_{\nu,m}(t)}{l}P(n-\nu+1,\vec{c}-\vec{\delta}_m,t)(1-\delta_{n,n_{\max}}\delta_{\nu,0})\\ &+ \sum_{m=1}^{M}\left[\left(\frac{c_m+1}{\tau_m}\right)P(n-1,\vec{c}+\vec{\delta}_m,t)(1-\delta_{c_m,c_{m,\max}}) - \left(\frac{c_m}{\tau_m}\right)P(n,\vec{c},t)\right]\\ &+ S(t)\Big(P(n-1,\vec{c},t) - P(n,\vec{c},t)\Big)\end{aligned} \tag{15}$$

The terms in (Eq. 15) are not included in the summations if they correspond to a neutron or precursor population that exceed the limits $n_{\max}$ and $c_{m,\max}$ respectively. The exclusive of terms that exceed $n_{\max}$ and $c_{m,\max}$ is necessary as a termination criterion. The limits, $n_{\max}$ and $c_{m,\max}$ were set as user-defined variables in order to reduce the computation time of specific systems being analysed. Consequently, the accuracy of the method decreases as the distribution of the probabilities shift towards the maximum allowable neutron populations. An example of this decrease in accuracy is shown in Appendix B.

The model provides a very accurate solution to the neutron population probability distribution function given that the probability that the population is equal to the maximum allowable neutron population is low. The accuracy and computational efficiency of the model will be compared to the other models.

2.3. *The Generating Function Form of the Forward Probability Balance Equations*

Bell [16] continued the forward probability balance model by introducing the probability generating function $F(x,\vec{y},t)$ where:

$$F(x,\vec{y},t) = \sum_{n=0}^{\infty}\sum_{c_1=0}^{\infty}\cdots\sum_{c_M=0}^{\infty}x^n y_1^{c_1}\cdots y_M^{c_M}P(n,\vec{c},t). \tag{16}$$

It is possible to then derive a PDE for F by multiplying both sides of (Eq.14) by $x^n y_1^{c_1} \cdots y_M^{c_M}$ and summing over $n, c_1, \cdots, c_M$ [30]:

$$\frac{\partial F(x,\vec{y},t)}{\partial t} = g(x,\vec{y},t)\frac{\partial F(x,\vec{y},t)}{\partial x} + \sum_{m=1}^{M} \lambda_m (x - y_m)\frac{\partial F(x,\vec{y},t)}{\partial y_m} + S(x-1)F(x,\vec{y},t). \tag{17}$$

(Eq. 17) can, after appropriate differentiation with respect to x and y_m, be evaluated at $x = y_m = 1$ to give moments of the probability distribution. (Eqs. 18-19) presented below are the first moment equations of the FGF model:

$$\frac{d\bar{n}(t)}{dt} = [\bar{\nu}(1-\beta)\lambda_f(t) - \lambda_a]\bar{n}(t) + \sum_{m=1}^{M} \lambda_m \bar{c}_m(t) + S \tag{18}$$

$$\frac{d\bar{c}_m(t)}{dt} = -\lambda_m \bar{c}_m(t) + \bar{\nu}\beta_m \lambda_f(t)\bar{n}(t) \tag{19}$$

where, $\bar{n}(t)$ is the mean neutron population, $\bar{c}_m(t)$ is the mean population for delayed neutron precursor group m, $\lambda_f = \nu\Sigma_f$, and $\lambda_a = \nu\Sigma_a$. The standard deviation in the neutron population can then be calculated by:

$$\sigma_N^2(t) = \mu_{NN}(t) + \bar{n}(t) - \bar{n}^2(t) \tag{20}$$

where,

$$\frac{d\mu_{NN}(t)}{dt} = 2S\bar{n}(t) + \lambda_f(t)\hat{\chi}_2\bar{n}(t) + 2\sum_{m=1}^{M} \lambda_m \mu_{Nm}(t) + 2[\bar{\nu}(1-\beta)\lambda_f(t) - \lambda_a(t)]\mu_{NN}(t) \tag{21}$$

$$\frac{d\mu_{Nk}(t)}{dt} = S\bar{c}_k(t) + \sum_{m=1}^{M} \lambda_m \mu_{Nk}(t) - \lambda_k \mu_{Nk}(t) + \bar{\nu}\beta_k \lambda_f(t)\mu_{NN}(t) + [\bar{\nu}(1-\beta)\lambda_f(t) - \lambda_a(t)]\mu_{Nk}(t) + \bar{\nu}(1-\beta)\bar{\nu}\beta_k\lambda_f(t)\bar{n}(t) \tag{22}$$

$$\frac{d\mu_{mk}(t)}{dt} = -(\lambda_m + \lambda_k)\mu_{mk}(t) + \bar{\nu}\lambda_f(t)(\beta_k\mu_{Nm} + \beta_m\mu_{Nk}) + \bar{\nu}\beta_m\bar{\nu}\beta_k\lambda_f(t)\bar{n}(t)(1-\delta_{mk}) \tag{23}$$

The derivation of these equations and definitions of each of the terms are shown in Appendix C. The FGF model will be used to generate the mean and standard deviation and serve as a verification tool for the other models in this study. The survival probability, extinction probability, and CDF will not be computed with this method. This is because there are complex numerical difficulties associated with the method which are explained in Appendix D.

However, it can be shown that distributions for highly multiplicative systems tend towards a gamma distribution. Therefore, it is possible to approximate the neutron CDF with the mean and standard deviation computed by the FGF model by using the gamma distribution approximation E.1. Williams and Eaton [11, 12] have shown that the gamma distribution is very accurate over the most prominent part of the distribution while the tails of the distribution differ significantly from the true solution. However, they demonstrated that the tails of the distribution are the most important region of the curve for low neutron source calculations such as nuclear reactor start-up. The use of the gamma approximation will be illustrated in Appendix E to demonstrate its numerical accuracy and computational efficiency.

2.4. *The Generating Function Form of the Backward Probability Balance Equations*

The Pál Bell equation has been used to model low neutron source problems in many studies [6, 11, 12, 13, 29]. A full mathematical derivation of the Pál-Bell equation is not presented in this paper. The Pál-Bell equation is rigorously derived and explained elsewhere within the literature [21, 22, 23]. However, the spatially-independent, mono-energetic, Pál Bell equation, implemented in this study, is presented. As only one neutron emission per extraneous neutron source disintegration has been considered in the study, the complexity of the Pál-Bell equation can be further reduced. The Pál Bell equation contains two sets of generating functions, the first in the absence of an extraneous neutron source $\tilde{G}(z,t|s)$ and the second with an extraneous neutron source $\tilde{G}_S(z,t|s)$.

(Eqs. 24-29) describe the generating functions, $\tilde{G}(z,t|s)$, $\tilde{G}_{dm}(z,t|s)$, and their first and second derivatives with respect to z. These generating functions correspond to the neutron population distribution at time t given the injection at earlier time s of a single neutron (Eqs. 24-26) or a single delayed neutron precursor in group m (Eqs. 27-29):

$$-\frac{1}{v}\frac{\partial \tilde{G}(z,t|s)}{\partial s} = -\Sigma_a(s)\tilde{G} + \Sigma_f(s) - \Sigma_f(s)H(\tilde{G},\tilde{G}_{dm}) \tag{24}$$

$$-\frac{1}{v}\frac{\partial \tilde{G}'(z,t|s)}{\partial s} = -\Sigma_a(s)\tilde{G}' - \Sigma_f(s)H'(\tilde{G},\tilde{G}_{dm}) \tag{25}$$

$$-\frac{1}{v}\frac{\partial \tilde{G}''(z,t|s)}{\partial s} = -\Sigma_a(s)\tilde{G}'' - \Sigma_f(s)H''(\tilde{G},\tilde{G}_{dm}) \tag{26}$$

$$-\frac{\partial \tilde{G}_{dm}}{\partial s} = \lambda_i(\tilde{G} - \tilde{G}_{dm}) \tag{27}$$

$$-\frac{\partial \tilde{G}'_{dm}}{\partial s} = \lambda_i(\tilde{G}' - \tilde{G}'_{dm}) \tag{28}$$

$$-\frac{\partial \tilde{G}''_{\mathrm{d}m}}{\partial s} = \lambda_i(\tilde{G}'' - \tilde{G}''_{\mathrm{d}m}) \tag{29}$$

where:

$$H(\tilde{G}, \tilde{G}_{\mathrm{d}m}) = \sum_{n=0}^{\nu_{\max}} \frac{(-1)^n}{n!}\chi_n \tilde{G}^n \prod_{m=1}^{M}(1 - \bar{\nu}\beta_m \tilde{G}_{\mathrm{d}m}) \tag{30}$$

$$\begin{aligned} H'(\tilde{G}, \tilde{G}_{\mathrm{d}m}) = &- \sum_{n=0}^{\nu_{\max}} \frac{(-1)^n}{n!}\chi_n \tilde{G}^n \sum_{m=1}^{M} \bar{\nu}\beta_m \tilde{G}'_{\mathrm{d}m} \prod_{k=1,k\neq m}^{M}(1 - \bar{\nu}\beta_k \tilde{G}_{\mathrm{d}k}) \\ &+ \sum_{n=1}^{\nu_{\max}} \frac{(-1)^n}{n!}\chi_n n \tilde{G}^{n-1}\tilde{G}' \prod_{m=1}^{M}(1 - \bar{\nu}\beta_m \tilde{G}_{\mathrm{d}m}) \end{aligned} \tag{31}$$

$$\begin{aligned} H''(\tilde{G}, \tilde{G}_{\mathrm{d}m}) = &\sum_{n=0}^{\nu_{\max}} \frac{(-1)^n}{n!}\chi_n \tilde{G}^n \sum_{m=1}^{M}\left(\bar{\nu}\beta_m \tilde{G}'_{\mathrm{d}m} \sum_{k=1,k\neq m}^{M} \frac{\bar{\nu}\beta_k \tilde{G}'_{\mathrm{d}k}}{1 - \bar{\nu}\beta_k \tilde{G}_{\mathrm{d}k}} \right. \\ &\left. \prod_{k=1,k\neq m}^{M}(1 - \bar{\nu}\beta_k \tilde{G}_{\mathrm{d}k})\right) \\ &- \sum_{n=0}^{\nu_{\max}} \frac{(-1)^n}{n!}\chi_n \tilde{G}^n \sum_{m=1}^{M}\left(\bar{\nu}\beta_m \tilde{G}''_{\mathrm{d}m} \prod_{k=1,k\neq m}^{M}(1 - \bar{\nu}\beta_k \tilde{G}_{\mathrm{d}k})\right) \\ &- \sum_{n=1}^{\nu_{\max}} \frac{(-1)^n}{n!}\chi_n 2n \tilde{G}^{n-1}\tilde{G}' \sum_{m=1}^{M}\left(\bar{\nu}\beta_m \tilde{G}''_{\mathrm{d}m} \prod_{k=1,k\neq m}^{M}(1 - \bar{\nu}\beta_k \tilde{G}_{\mathrm{d}k})\right) \\ &+ \sum_{n=1}^{\nu_{\max}} \frac{(-1)^n}{n!}\chi_n n \tilde{G}^{n-1}\tilde{G}'' \prod_{m=1}^{M}(1 - \bar{\nu}\beta_m \tilde{G}_{\mathrm{d}m}) \\ &+ \sum_{n=2}^{\nu_{\max}} \frac{(-1)^n}{n!}\chi_n n(n-1) \tilde{G}^{n-2}\tilde{G}'^2 \prod_{m=1}^{M}(1 - \bar{\nu}\beta_m \tilde{G}_{\mathrm{d}m}). \end{aligned} \tag{32}$$

(Eqs. 33-35) are solved for $G_s(z, t|s)$ and its derivatives with respect to z. This is the generating function related to the neutron population distribution at time t due to the neutrons released by the neutron source between time s and time t. This system of equations are solved backwards in time from $s = t$ to $s = 0$:

$$\frac{\partial G_{\mathrm{s}}(z, t|s)}{\partial s} = S(s) G_{\mathrm{s}} \tilde{G}^n \tag{33}$$

$$\frac{\partial G'_{\mathrm{s}}(z, t|s)}{\partial s} = S(s)\left(\tilde{G}G'_{\mathrm{s}} + \tilde{G}'G_{\mathrm{s}}\right) \tag{34}$$

$$\frac{\partial G''_{\mathrm{s}}(z, t|s)}{\partial s} = S(s)\left(\tilde{G}G''_{\mathrm{s}} + 2\tilde{G}'G'_{\mathrm{s}} + \tilde{G}''G_{\mathrm{s}}\right). \tag{35}$$

(Eqs. 36-44) describe the final conditions for (Eqs. 24-35).

$$\tilde{G}(z, t|t) = 1 - z \tag{36}$$

$$\tilde{G}'(z, t|t) = -1 \tag{37}$$

$$\tilde{G}''(z, t|t) = 0 \tag{38}$$

$$\tilde{G}_{\mathrm{d}m}(z, t|t) = 0 \tag{39}$$

$$\tilde{G}'_{\mathrm{d}m}(z, t|t) = 0 \tag{40}$$

$$\tilde{G}''_{\mathrm{d}m}(z, t|t) = 0 \tag{41}$$

$$\tilde{G}_{\mathrm{S}}(z, t|t) = 1 \tag{42}$$

$$\tilde{G}'_{\mathrm{S}}(z, t|t) = 0 \tag{43}$$

$$\tilde{G}''_{\mathrm{S}}(z, t|t) = 0 \tag{44}$$

2.4.1. The Extinction Probability and Survival Probability

The extinction probability, P_{E}, can be calculated from the generating function, $G_{\mathrm{s}}(z, t|s)$. This can be derived from the definition of the generating function:

$$G_{\mathrm{s}}(z, t|s) = \sum_{n=0}^{\infty} z^n P(n, t|s). \tag{45}$$

Thus,

$$G_{\mathrm{s}}(t|s)\Big|_{z=0} = P(0, t|s) = P_{\mathrm{E}}(t - s). \tag{46}$$

As discussed earlier, the definition of the survival probability in this study is the probability that there is at least one neutron in the system in the absence of an external neutron source. As such, the survival probability P_{S} can be calculated viz:

$$1 - \tilde{G}(t|s)\Big|_{z=0} = 1 - P(0, t|s) = P_{\mathrm{S}}(t - s). \tag{47}$$

2.4.2. The Mean and Variance

The mean neutron population, $\bar{N}_{\mathrm{S}}(t|s)$, and variance, $\sigma^2_{\mathrm{S}}(t|s)$, can be calculated from the generating function $G'_{\mathrm{s}}(z, t|s)$, and $G''_{\mathrm{s}}(z, t|s)$ viz:

$$\tilde{G}'_{\mathrm{s}}(t|s)\Big|_{z=1} = \bar{N}_{\mathrm{S}}(t|s) \tag{48}$$

$$\tilde{G}''_{\mathrm{s}}(t|s)\Big|_{z=1} = \langle N(N-1)\rangle_{\mathrm{s}}(t|s) \tag{49}$$

thus,

$$\sigma^2_{\mathrm{S}}(t|s) = \tilde{G}''_{\mathrm{s}}(t|s)\Big|_{z=1} + \tilde{G}'_{\mathrm{s}}(t|s)\Big|_{z=1} - \tilde{G}'^2_{\mathrm{s}}(t|s)\Big|_{z=1} \tag{50}$$

where $\bar{N}_S$ and σ_S are the mean neutron population and standard deviation when a neutron source is present.

2.4.3. The Cumulative Distribution Function

The probability, $Q(n^*, t|s)$, that there are fewer than $n*$ neutrons in the system at time t can be calculated by solving the saddle-point method [11]:

$$Q(n^*, t|s) = \frac{1}{\sqrt{2\pi\sigma_0}} \frac{G_s(z_0, t|s)}{z_0^{n^*}(1 - z_0)} \tag{51}$$

where

$$\sigma_0 = \frac{n^*}{z_0^2} + \frac{1}{(1 - z_0)^2} - \left(\frac{G_s'(z_0, t|s)}{G_s(z_0, t|s)}\right)^2 + \frac{G_s''(z_0, t|s)}{G_s(z_0, t|s)} \tag{52}$$

where z_0 is given as the root of the equation:

$$\frac{n^*}{z_0} = \frac{1}{(1 - z_0)} + \frac{G_s'(z_0, t|s)}{G_s(z_0, t|s)}. \tag{53}$$

The neutron population CDF can be constructed by solving the generating functions backwards in time while varying the input $0 \leq z < 1$. It is known that the saddle-point method tends to the wrong limit for $n^* >> \bar{N}_S$; with the saddle-point method $Q(n^*, t|s)$ tends to $\frac{e}{\sqrt{2\pi}} = 1.08444...$ instead of tending to 1.0 [31]. However, the saddle-point method has been shown to be very accurate in the probability range that is relevant for low source startup calculations, namely $10^{-5} < Q < 10^{-8}$, when the mean neutron population is very large [11].

2.5. The Itô Calculus Model

Stochastic fluctuations can be introduced into the deterministic neutron kinetics equations by adding numerically generated noise into the terms of the equations. This allows the resultant equations to model stochastic phenomena. An Itô calculus approach can be derived from the deterministic neutron kinetics equations in the following form [26]:

$$\begin{aligned}
\frac{\mathrm{d}\bar{n}(t)}{\mathrm{d}t} &= -\left[\frac{-\rho(t) + 1 - \alpha}{l}\right]\bar{n}(t) + \left[\frac{1 - \alpha - \beta}{l}\right]\bar{n}(t) + \sum_{m=1}^{M} \lambda_m \bar{c}_m(t) + S \\
\frac{\mathrm{d}\bar{c}_m(t)}{\mathrm{d}t} &= \frac{\beta_m}{l}\bar{n}(t) - \lambda_m \bar{c}_m(t)
\end{aligned} \tag{54}$$

where $\rho(t)$ is the reactivity as a function of time, $\alpha = \Sigma_\mathrm{f}/(\Sigma_\mathrm{a} k_\infty)$, and k_∞ is the infinite multiplication factor.

2.5.1. Derivation of One-Precursor Group Stochastic Neutron Point Kinetic Model

Following the method by Ray [26], the derivation of the one delayed neutron precursor group stochastic neutron kinetic equations will be shown and then an arbitrary precursor group model will be shown. The equations shown below have been written with the same notation as the other models in this study. The deterministic neutron kinetics equations for one delayed neutron precursor group is given by:

$$\begin{aligned}
\frac{\mathrm{d}\bar{n}(t)}{\mathrm{d}t} &= -\left[\frac{-\rho(t) + 1 - \alpha}{l}\right]\bar{n}(t) + \left[\frac{1 - \alpha - \beta}{l}\right]\bar{n}(t) + \lambda_1 \bar{c}_1(t) + S \\
\frac{\mathrm{d}\bar{c}_1(t)}{\mathrm{d}t} &= \frac{\beta_1}{l}\bar{n}(t) - \lambda_1 \bar{c}_1(t)
\end{aligned} \tag{55}$$

Similar to the FPB method (Eq.13), the Itô calculus approach for modelling the stochastic behaviour of neutrons can be constructed by listing all possible neutronic events. Let:

1. E_1 be the first event, representing a neutron capture;
2. E_2 the second event, representing a fission event;
3. E_3 the third event, representing the transformation of a delayed neutron precursor to a neutron;
4. E_4 the fourth event, representing the emission of a neutron from a neutron source.

The change incurred to the population of neutrons n and delayed precursor c_1 for each event is then:

$$E_1 \begin{bmatrix} dn \\ dc_1 \end{bmatrix}_1 = \begin{bmatrix} -1 \\ 0 \end{bmatrix}$$

$$E_2 \begin{bmatrix} dn \\ dc_1 \end{bmatrix}_2 = \begin{bmatrix} -1 + (1 - \beta_1)\overline{\nu} \\ \beta_1 \overline{\nu} \end{bmatrix}$$

$$E_3 \begin{bmatrix} dn \\ dc_1 \end{bmatrix}_3 = \begin{bmatrix} 1 \\ -1 \end{bmatrix}$$

$$E_4 \begin{bmatrix} dn \\ dc_1 \end{bmatrix}_4 = \begin{bmatrix} 1 \\ 0 \end{bmatrix}$$

where $E_k[dn\ dc_1]_j^T$ is the expected change in the neutron and precursor populations due to event j occurring. The probability of these four events occurring are:

$$P(E_1) = n\nu\Sigma_\mathrm{c} dt$$

$$P(E_2) = n\nu\Sigma_\mathrm{f} dt$$

$$P(E_3) = c_1\lambda_1 dt$$

$$P(E_4) = S\, dt$$

where the dn is the change in the neutron population and dc_1 is the change in the precursor population. It should be noted that these events correspond to individual particle histories and not the mean populations. As such, the changes occur to the neutron population n and not the mean neutron population $\bar{n}$.

The mean change in a small time interval dt is then:

$$E\left\{\begin{bmatrix} dn \\ dc_1 \end{bmatrix}\right\} = \sum_{j=1}^{4} P_j \begin{bmatrix} dn \\ dc_1 \end{bmatrix}_j = \begin{bmatrix} \frac{\rho-\beta}{l} n + \lambda_1 c_1 + S \\ \frac{\beta_1}{l} n - \lambda_1 c_1 \end{bmatrix} dt$$

and the variance in a small time dt is

$$\begin{aligned}
Var\left\{\begin{bmatrix} dn \\ dc_1 \end{bmatrix}\right\} &= \left\{\begin{bmatrix} dn \\ dc_1 \end{bmatrix}\begin{bmatrix} dn & dc_1 \end{bmatrix}\right\} - \left\{E\left(\begin{bmatrix} dn \\ dc_1 \end{bmatrix}\right)\right\}^2 \\
&= \sum_{j=1}^{4} P_j \begin{bmatrix} dn \\ dc_1 \end{bmatrix}_j \begin{bmatrix} dn & dc_1 \end{bmatrix}_j = \hat{B} dt
\end{aligned}$$

where $P_j = P(E_j)$ and $\hat{B}$ is a (2×2) matrix containing n, c_1, and S. From the central limit theorem, the mean and variance

of the neutron population can be related to a standard normal distribution via the random variate:

$$\left\{\begin{bmatrix} dn \\ dc_1 \end{bmatrix} - E\left(\begin{bmatrix} dn \\ dc_1 \end{bmatrix}\right)\right\} \Big/ \sqrt{Var\left(\begin{bmatrix} dn \\ dc_1 \end{bmatrix}\right)} \tag{56}$$

The above result generates the following equation:

$$\begin{bmatrix} dn \\ dc_1 \end{bmatrix} = E\left(\begin{bmatrix} dn \\ dc_1 \end{bmatrix}\right) + \sqrt{Var\left(\begin{bmatrix} dn \\ dc_1 \end{bmatrix}\right)} \begin{bmatrix} \epsilon_1 \\ \epsilon_2 \end{bmatrix}, \qquad \text{where} \quad \epsilon_1, \epsilon_2 \sim N(0,1) \tag{57}$$

Thus producing:

$$\begin{bmatrix} n(t+dt) \\ c_1(t+dt) \end{bmatrix} = \begin{bmatrix} n(t) \\ c_1(t) \end{bmatrix} + \begin{bmatrix} \frac{\rho-\beta}{l} n + \lambda_1 c_1 \\ \frac{\beta_1}{l} n - \lambda_1 c_1 \end{bmatrix} dt + \begin{bmatrix} S \\ 0 \end{bmatrix} dt + \hat{B}^{1/2} \sqrt{dt} \begin{bmatrix} \epsilon_1 \\ \epsilon_2 \end{bmatrix} \tag{58}$$

This is the stochastic point neutron kinetics equations with one group of delayed neutron precursor groups, which can be extended to include an arbitrary number of precursor groups and is shown in the following section.

2.5.2. *Multiple Precursor Groups*

Following a similar procedure as that shown above the following result can be derived:

$$\frac{\mathrm{d}\vec{x}}{\mathrm{d}t} = A\vec{x} + B(t)\vec{x} + \vec{F}(t) + \hat{B}^{1/2} \frac{\mathrm{d}\overline{W}}{\mathrm{d}t} \tag{59}$$

where:

$$\vec{x} = \begin{bmatrix} n \\ c_1 \\ c_2 \\ \vdots \\ c_M \end{bmatrix} \tag{60}$$

$$A = \begin{bmatrix} \frac{-\beta}{l} & \lambda_1 & \lambda_2 & \cdots & \lambda_M \\ \frac{\beta_1}{l} & -\lambda_1 & 0 & \cdots & 0 \\ \frac{\beta_2}{l} & 0 & -\lambda_2 & \ddots & \vdots \\ \vdots & \vdots & \ddots & \ddots & 0 \\ \frac{\beta_M}{l} & 0 & \cdots & 0 & -\lambda_M \end{bmatrix} \tag{61}$$

$$B = \begin{bmatrix} \frac{\rho(t)}{l} & 0 & 0 & 0 & 0 \\ 0 & 0 & 0 & \cdots & 0 \\ 0 & 0 & 0 & \ddots & \vdots \\ \vdots & \vdots & \ddots & \ddots & 0 \\ 0 & 0 & \cdots & 0 & 0 \end{bmatrix} \tag{62}$$

$$\vec{F}(t) = \begin{bmatrix} S(t) \\ 0 \\ 0 \\ \vdots \\ 0 \end{bmatrix} \tag{63}$$

$$\hat{B} = \begin{bmatrix} \zeta & a_1 & a_2 & \cdots & a_M \\ a_1 & r_1 & b_{2,3} & \cdots & b_{2,M+1} \\ a_2 & b_{3,2} & r_2 & \ddots & \vdots \\ \vdots & \vdots & \ddots & \ddots & b_{M,M+1} \\ a_M & b_{M+1,2} & \cdots & b_{M+1,M} & r_M \end{bmatrix} \tag{64}$$

where

$$\zeta = \gamma n + \sum_{m=1}^{M} \lambda_m c_m + S \tag{65}$$

$$\gamma = \frac{-1 - \rho + 2\beta + (1-\beta)^2 \overline{\nu}}{l} \tag{66}$$

$$a_m = \frac{\beta_m}{l}[-1 + (1-\beta)\overline{\nu}]n - \lambda_m c_m \tag{67}$$

$$b_{m,k} = \frac{\beta_{m-1}\beta_{k-1}\overline{\nu}}{l} n \tag{68}$$

and

$$r_m = \frac{\beta_m^2 \overline{\nu}}{l} n + \lambda_m c_m \tag{69}$$

The Wiener process term, $d\overline{W}_i$, is the stochastic term of (Eq.59) making the expression a SDE rather than an ODE. Applying the explicit Euler-Maruyama method to (Eq.59), the simplest time discrete approximation of an Itô calculus process can be written as [26]:

$$\vec{x}_{i+1} = \vec{x}_i + (A + B_i)\vec{x}_i h + \vec{F}(t_i)h + \hat{B}^{1/2} \sqrt{h}\vec{\epsilon}_i \tag{70}$$

where $\sqrt{h}\vec{\epsilon}_i = d\vec{W}_i$, $h = t_{i+1} - t_i$, and $\vec{\epsilon}_i$ is a vector whose components are random numbers generated from a normal distribution $N(0,1)$. (Eq.70) can conceptually be considered a continuous version of the AMC model, whereby random numbers are generated to determine the evolution of the system and requires thousands of realisations to accurately describe the system.

The generation of the different numerical results and quantities of interest (QoI) from the Itô calculus model require a different technique. A running total of x, x^2, and $x = 0$ are taken for each time increment. Once the total number of realisations have been performed, $E[x]$, $E[x^2]$, $E[x = 0]$ are readily computed allowing for the generation of the mean, standard deviation, and survival probability. The extinction probability and cumulative distribution function require the continuous variable, x, to be discretized. At time t, the variable x is discretized, and +1 is added to the cell in an array that corresponds to that population and moment in time. This array is added to across all realisations which can then be used to calculate the CDF. A separate array is used for the calculation of the extinction probability which is explained in Appendix H.

Suescún-Díaz [28] has further improved the method by developing an implicit Euler-Maruyama discretization scheme in the form of:

$$\hat{P}_{i+1} = S^{-1}(\hat{P}_i + \hat{Q}_{i+1}h + B_i^{1/2}d\vec{W}_i) \tag{71}$$

where,

$$S = (I - A_{i+1}h) \tag{72}$$

$$S^{-1} = (I - A_{i+1}h)^{-1} = \begin{bmatrix} s_{1,1} & s_{1,2} & s_{1,3} & \cdots & s_{1,M+1} \\ s_{2,1} & s_{2,2} & s_{2,3} & \cdots & s_{2,M+1} \\ s_{3,1} & s_{3,2} & s_{3,3} & \cdots & s_{3,M+1} \\ \vdots & \vdots & \vdots & \ddots & \vdots \\ s_{M+1,1} & s_{M+1,2} & s_{M+1,3} & \cdots & s_{M+1,M+1} \end{bmatrix} \tag{73}$$

where,

$$s_{1,k} = \frac{1}{\zeta_{i+1}}\left[1 + (1-\delta_{1,k})\left(\frac{\lambda_{k-1}h}{1+\lambda_{k-1}h} - 1\right)\right] \quad \text{for } k = 1, ..., M+1 \tag{74}$$

$$s_{m,k} = \frac{1}{1+\lambda_{m-1}h}\left(\delta_{m,k} + \frac{\beta_{m-1}h}{l}s_{1,k}\right) \quad \text{for } m = 2, ..., M+1 \quad k = 1, ..., M+1 \tag{75}$$

where

$$\zeta_{i+1} = 1 - \left[\frac{\rho(t_{i+1}) - \beta}{l}\right]h - \frac{h^2}{l}\left(\sum_{m=1}^{M}\frac{\lambda_m\beta_m}{1+\lambda_m ih}\right). \tag{76}$$

Both the explicit and implicit Euler-Maruyama discretization schemes have been modelled in this paper.

2.6. Temporal discretization and the Number of Realisations

In total, five models have been developed for comparison:

1. Analog Monte-Carlo (AMC)
2. Forward probability balance equations (FPB)
3. Generating function form of the forward probability balance equations (FGF)
4. Generating function form of the backward probability balance equations or Pál-Bell (PB)
5. Itô Calculus
   (a) Explicit Euler-Maruyama discretization (EEM)
   (b) Implicit Euler-Maruyama discretization (IEM)

The accuracy of certain models developed in this study are dependent on the temporal discretization, number of realisations, or maximum neutron population allowable in the simulation Therefore, two methods of numerical comparison are available. The first option is run each model until it has fully converged to a solution and compare the accuracy, required temporal discretization, number or realisations, and maximum population required. The second option is to select a temporal discretization, number of realisations, and maximum neutron population and compare the accuracy of each model and degree of convergence. The second option has been chosen in this study. Table 2 shows the values chosen for each model.

Table 2: The temporal discretization, number of realisations, and maximum allowable neutron population used in each of the models developed in this study.

Method	Δt(s)	Realisations	Max Population
AMC	Variable	50,000	1000
FPB	ODE solver	/	100[1]
FGF	ODE solver	/	/
PB	ODE solver	/	/
EEM	1.0E-5	50,000	1000
IEM	1.0E-5	50,000	1000

As discussed previously, the discrete or continuous nature of these models lend themselves to the generation of different numerical results and quantities of interest (QoI). While it it possible to extract discrete data from the Pál-Bell model, approximations are required for the Itô-calculus model. The results that each model has been used to construct is shown in Table 3.

Table 3: The results that each model has been used to construct.

Method	Survival	Extinction	Moments	CDF
AMC	✓	✓	✓	✓
FPB	✓	✓	✓	✓
FGF	✗	✗	✓	✗
PB	✓	✓	✓	✓
EEM	✓	✓	✓	✓
IEM	✗	✗	✓	✗

The forward generating function method developed in this study only contains the moment equations. Therefore, this method has only been used to calculate the mean and standard deviation. This method has been included as the numerical accuracy of the forward probability balance method is limited by the maximum number of neutrons the model contains.

The Implicit Euler-Maruyama discretization model included in this study has only been used to calculate the mean and standard deviation. This is because the discretization scheme appears to limit the neutron population fluctuations. As a result, the method is much more accurate at modelling the mean neutron population but is no longer able to generate results regarding discrete entities such as the survival or extinction probabilities.

3. Modelling Stochastic Neutron Kinetics in the Absence of Delayed Neutron Precursors

It is most common to model systems that contain at least one group of delayed neutron precursors. However, comparing the numerical accuracy and computational efficiency of the different models in the absence of any delayed neutron precursor

[1] The maximum allowable delayed neutron precursor population for group m was set to $c_{m,\max} = n_{\max}\beta_m/\lambda_m$ rounded up to the nearest integer.

Table 4: The simulation time (s) for each method to compute the relevant numerical result when modelling zero groups of delayed neutron precursors. The survival probability simulation times are represented by the columns $S = 0$ as these simulations do not include an external neutron source. All models, excluding the Pál-Bell model, computed the extinction probability, moments, and cumulative distribution results at the same time and are represented by the columns $S = 5$ and $S = 5000$.

	S = 0		**S = 5**		**S = 5000**	
Method	**k = 0.9**	**k = 1.1**	**k = 0.9**	**k = 1.1**	**k = 0.9**	**k = 1.1**
PB	9E-2	8E-2	4E-2	4E-2	4E-2	5E-2
FPB	5E2	5E2	5E2	5E2	6E2	5E2
FGF	/	/	4E-4	2E-3	9E-4	1E-3
AMC	3E2	3E2	2E2	2E2	3E2	3E2
EEM	1E2	2E2	2E2	2E2	1E2	1E2
IEM	/	/	3E2	3E2	3E2	3E2

groups provides a relatively simple starting point.

Each mathematical model explained in Section 2 will be used to compute a range of results for constant reactivity systems which are either sub-critical ($k_{\text{eff}} = 0.9$) or super-critical ($k_{\text{eff}} = 1.1$). An external neutron source of either 5 n/s or 5000 n/s will be present. The simulation time required for each model to produce the relevant results in Section 3 is shown in Table 4.

3.1. The Survival Probability

The first comparison of the methods was their ability to calculate the survival probability (explained in Section 1). The results are shown in Figure 1. Good agreement can be seen across the PB, FPB, and AMC models for both the sub-critical and super-critical case.

In the case of the sub-critical simulation, the EEM method is able to approximately calculate the survival probability, while in the super-critical simulation it is not. The reduced accuracy of the EEM method is expected at higher reactivities and is illustrated in Appendix F. It is clear from Table 4 that the computational efficiency of the PB model is far superior than the other three models.

3.2. Extinction Probability

The next set of comparisons are the extinction probability (explained in Section 1). The results can be seen in Figure 2.

There is good agreement between the PB, FPB, and AMC models when calculating the extinction probability. The good agreement between these three models for the survival and extinction probability is to be expected. Both the AMC and FPB models have an upper-limit of the number of neutrons that they are able to simulate. This limitation of the models is directly linked to the computational efficiency of the numerical methods used in the models. However, as these results are mostly concerned with the numerical accuracy of the models at simulating low neutron populations, as long as the probability that the population has reached its maximum is small, then the numerical accuracy of these two models will not be affected significantly.

The extinction probability calculated by the the EEM method has not been included for the simulation with an external neutron source of 5 n/s. This is because the extinction probability calculated was too small to offer a meaningful comparison between the results.

The inaccuracy of the EEM method can be attributed to the continuous nature of the model. Unlike the AMC and FPB mod-

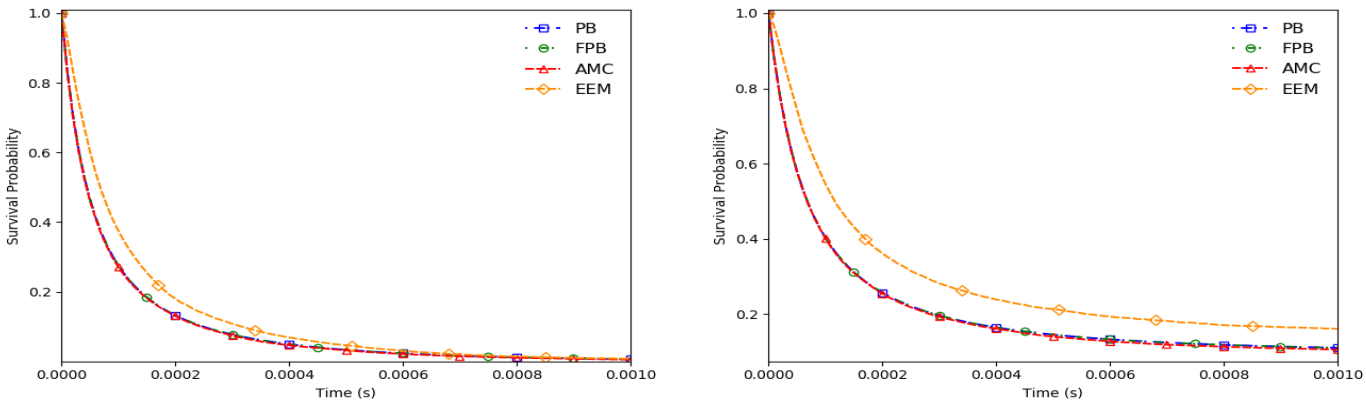

(a) (b)

Figure 1: The survival probability calculated by each model when including zero neutron precursor groups for the sub-critical case (a) and the super-critical case (b).

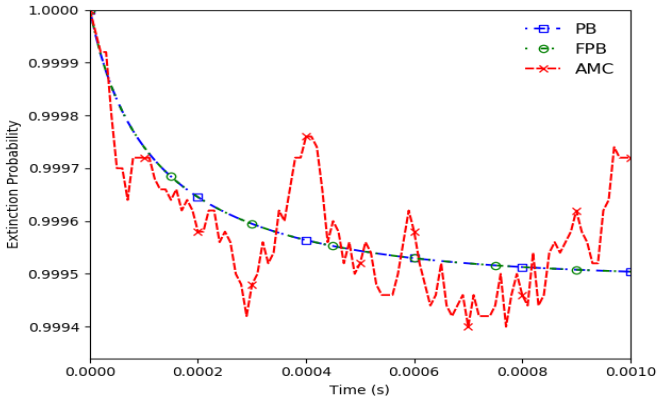

(a) External neutron source: 5 n/s.

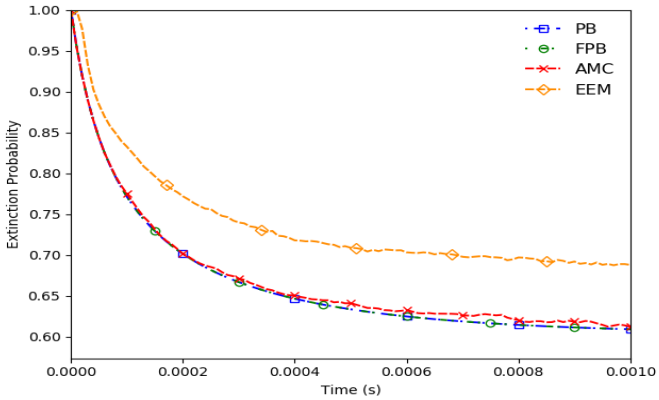

(b) External neutron source: 5000 n/s.

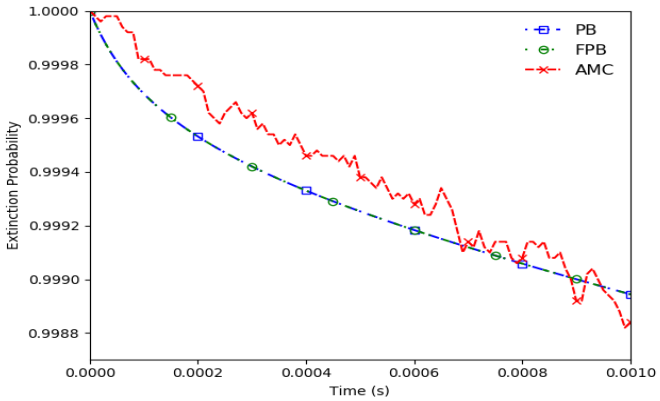

(c) External neutron source: 5 n/s.

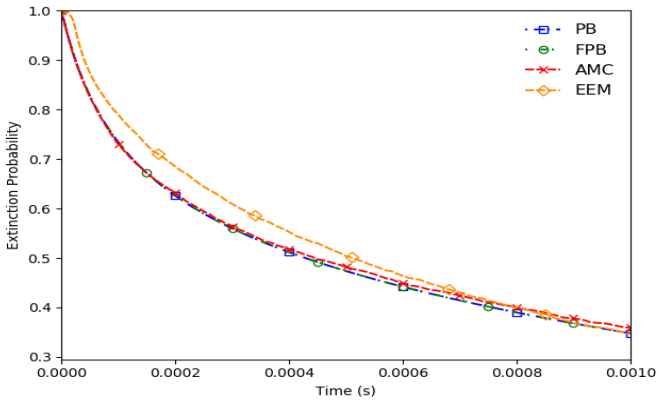

(d) External neutron source: 5000 n/s.

Figure 2: The extinction probability calculated by each model when including zero neutron precursor groups for the sub-critical case (a)(b) and the super-critical case (c)(d).

els, the EEM method produces a continuous neutron population while the result is concerned with an integer population. Unlike the PB model, there is no way to extract the extinction probability from its equation. Therefore, the neutron populations generated by the EEM method require disctretizing. For example, if the neutron population is 0.25, there exists a few options for how to deal with this value (rounded to the nearest integer, rounded down, or a distribution approach). The different disctretization methods tried are explained in Appendix H. Regardless of the discretization method implemented, the need for such a method introduces an approximation into the result. The results presented in this study indicate that the EEM method is not suitable for calculations of such a discrete nature. It should be noted that the EEM method produces results with much less variability for the system modelling an extraneous neutron source of 5000 n/s, however, good agreement with the other models is still not achieved. Again, it is clear that the PB model is the most computationally efficient and is not hindered by the fact the problem involves a low extraneous neutron source.

3.3. Cumulative Distribution Function (CDF)

The population cumulative density function is compared next. The results for the system with an extraneous source of 5000 n/s are shown in Figures 3. These results were extracted along with the same simulation set as the extinction probability calculations.

The AMC and FPB models show good agreement which is expected as they are both discrete methods. However, it can be seen in Figure 3 that the AMC model computes a marginally greater probability than the FPB model for low neutron populations. The comparison of the Figures 3a-3b indicate that the difference between the two models increases as the external neutron source increases. More accurately, this occurs due to the increasing neutron population. This is to be expected with the approximation required for the FPB model when modelling the upper limit of neutron populations.

It can be seen in Figure 3 that the saddle-point method used to generate the CDF from the PB model is not accurate at such a low neutron population. Referring to the work of Williams [11, 12], it is known that the saddle-point approximation becomes increasingly more accurate as $\frac{n_{\text{prob}}}{\bar{n}}$ increases. Comparing

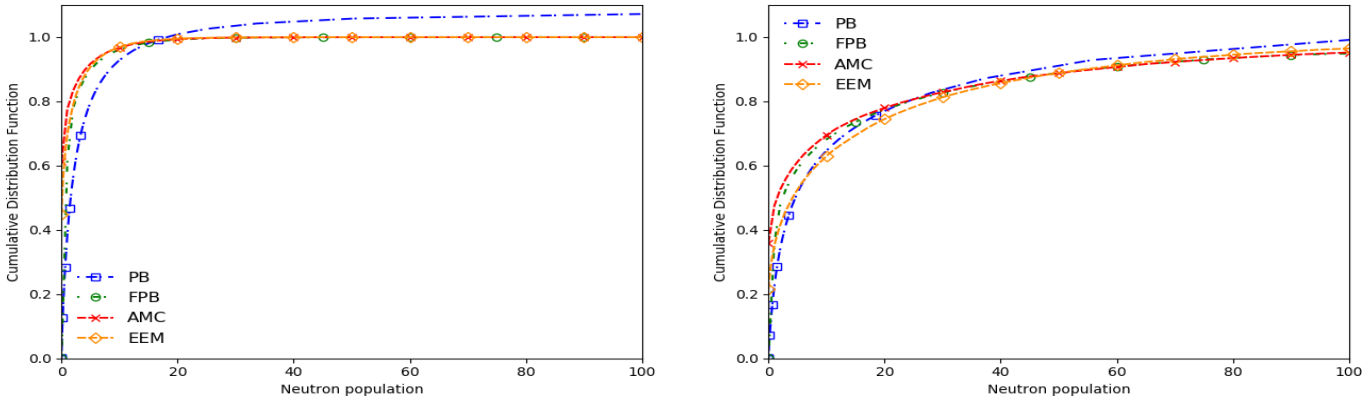

Figure 3: The cumulative distribution calculated by each model when including zero neutron precursor groups and an external neutron source of 5000 n/s for the sub-critical case (a) and the super-critical case (b). The CDF is computed at time $t = 100$ ms.

Figure 3a and 3b shows that as the neutron population increases, so does the agreement of the saddle-point approximation to the AMC and FPB models. This result is consistent with the work of Cooling [1], in which the saddle-point method was not applied until the maturity time of the system, at which point the neutron population was relatively large.

The EEM method is able to simulate a much higher neutron population than either the AMC or FPB model due to its continuous nature. Therefore, if the cumulative distribution is required where the mean neutron population is large then it is a more favourable method than either the AMC or FPB model. The EEM method shows good agreement with both the AMC and FPB model for the sub-critical case. Good agreement between these methods is also seen for the super-critical case once the neutron population has started to increase. This decrease in accuracy of the EEM method in modelling the cumulative distribution at low neutron populations for super-critical systems illustrates why the method is less accurate when computing the survival/extinction probability for the super-critical systems.

3.4. Population Mean and Standard Deviation

The mean and standard deviation of the neutron population is modelled next and the results are shown in Figures 4-5. These results are the first comparisons that contain all five models described in this study and offer the best insight into their differences.

Excellent agreement between the PB, FPB, and FGF models can be seen across all results for sub-critical systems. This result is to be expected as they are all exact models. There is an approximation required for the FPB model, however, as the neutron population mean and standard deviation in these sub-critical systems are very small, the FPB model is still very accurate.

The FPB model decreases in accuracy when modelling super-critical systems. It can be seen that both the mean and standard deviation calculated by the FPB model initially agree with results of the PB and FGF models for the super-critical systems. However, as the neutron population starts to increase, so does the numerical error in the model. This can be attributed to the model having a prescribed maximum allowable number of neutrons it can simulate. Effectively, the neutron population cannot exceed this prescribed maximum allowable number of neutrons meaning the higher neutron populations associated with the super-critical system can not be simulated.

The FGF model shows the importance of generating functions when modelling large numbers of neutrons. The model effectively condenses an infinite number of ODEs into a finite set of ODEs and is thus able to model super-critical systems and neutron populations which the FPB model would not be able to model with reasonable computational efficiency and numerical accuracy.

The AMC model shows good agreement with the PB and FGF models at the start of the simulation. However, as time increases, the differences between the numerical results and quantities of interest (QoI) start to increase. This is especially prevalent for the standard deviation. This result is expected because the variance in the neutron population increases in time. Therefore, it follows that there will be a greater variability between realisations as time increases. Thus, in order to maintain the same numerical accuracy in the result as time increases, an increasing number of realisations are needed. However, a set number of realisations was selected in order to illustrate a fair comparison between all computational models requiring realisations. The relative error of the AMC model is shown to decrease as the average number of neutrons in the system at any one time increases.

It can be seen that the EEM method is less accurate in modelling the mean and standard deviation than the AMC model

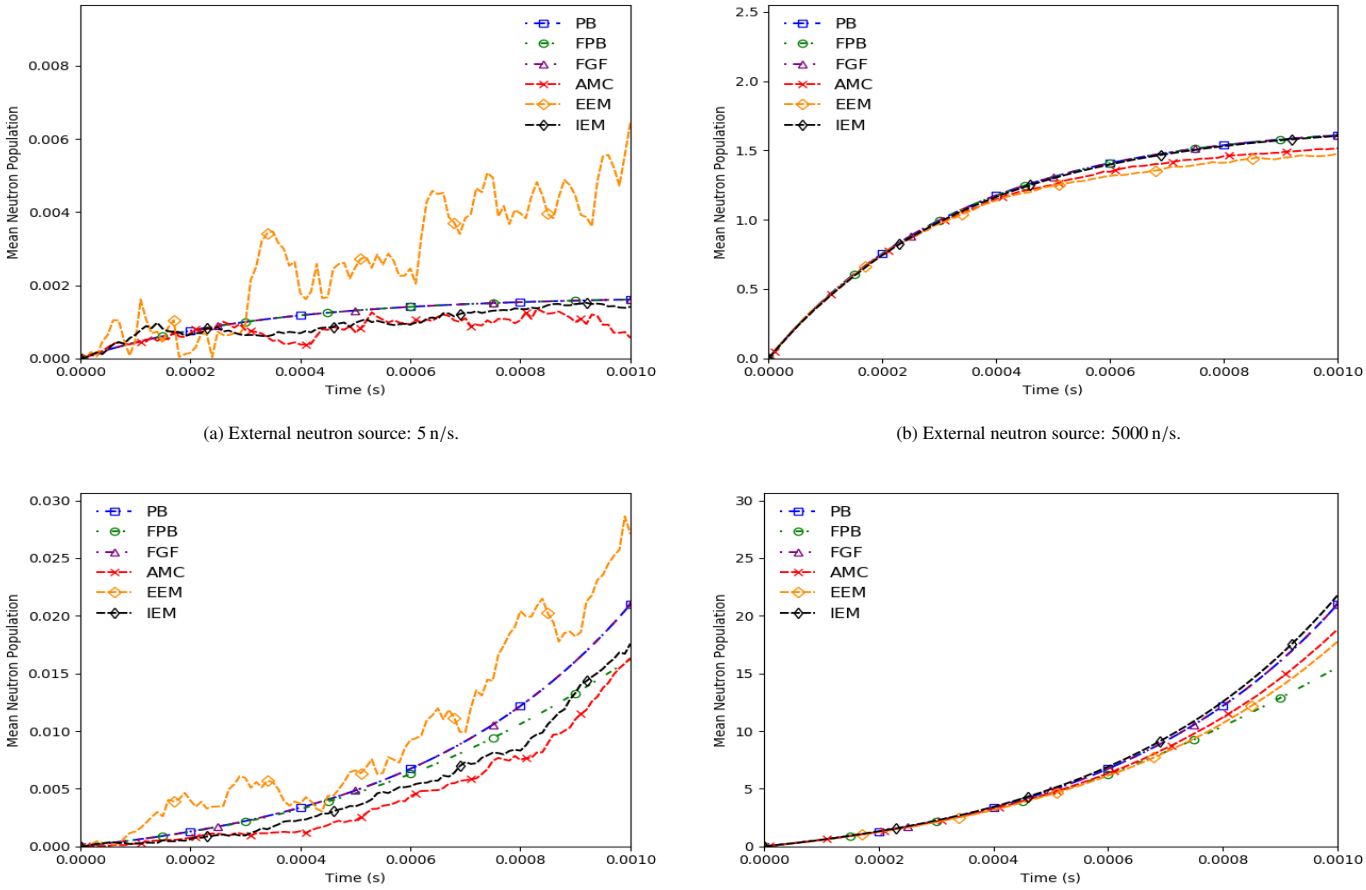

(a) External neutron source: 5 n/s.

(b) External neutron source: 5000 n/s.

(c) External neutron source: 5 n/s.

(d) External neutron source: 5000 n/s.

Figure 4: The mean neutron population calculated by each model including when zero neutron precursor groups for the sub-critical case (a)(b) and the super-critical case (c)(d).

when using the same number of realisations. The same decrease in numerical accuracy with time can be seen in this method as explained with the AMC model. The EEM method shows poor agreement with the other models for the sub-critical results with an external neutron source of 5 n/s. The numerical accuracy of the method in modelling the mean neutron population increases when the external neutron source is increased to 5000 n/s or the system is super-critical. However, the method appears to be incapable of accurately modelling the standard deviation in all scenarios.

The IEM method shows a much better agreement with the other models than the explicit EEM method when modelling the mean neutron population. However, the increased accuracy of the IEM method compared to the EEM method appears to come at the cost of a significant under-estimation of the standard deviation.

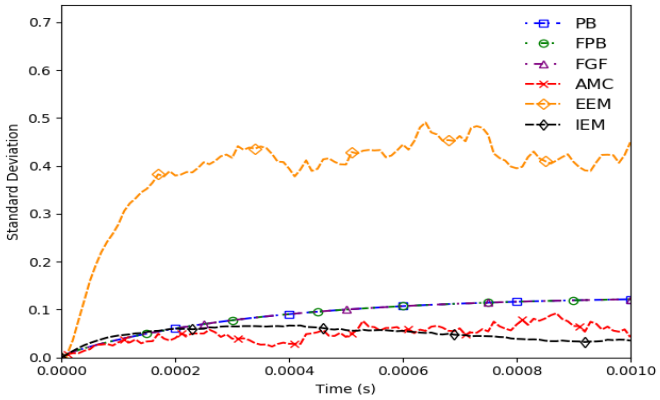

(a) External neutron source: 5 n/s.

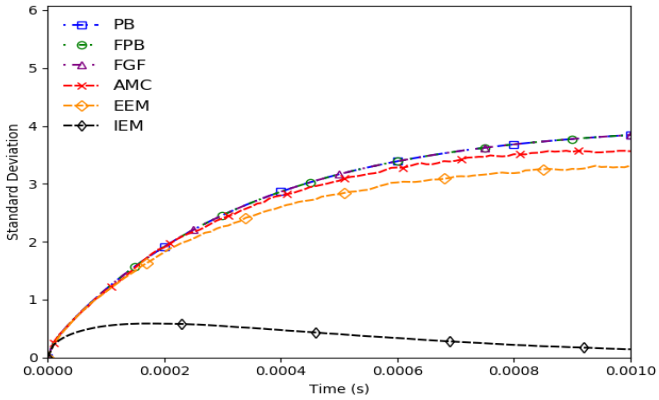

(b) External neutron source: 5000 n/s.

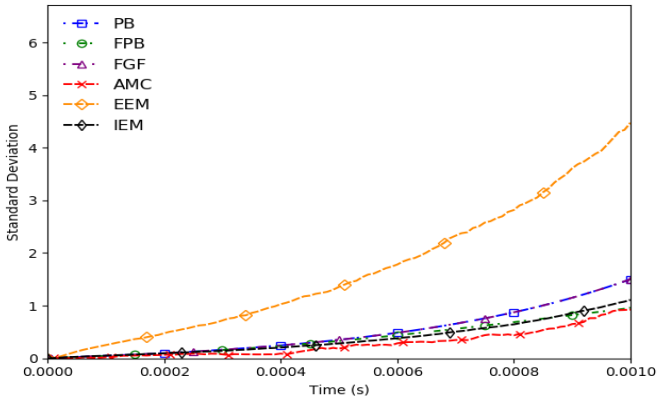

(c) External neutron source: 5 n/s.

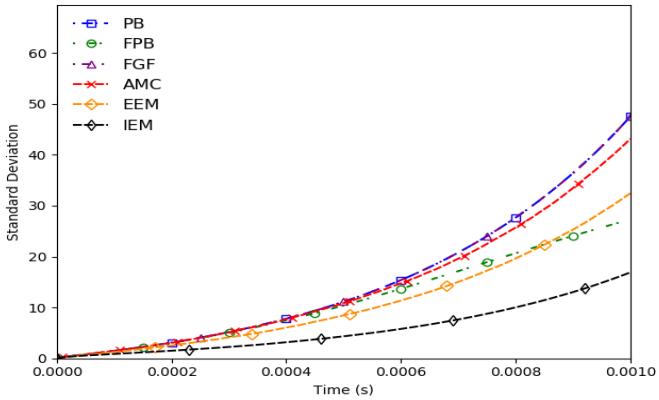

(d) External neutron source: 5000 n/s.

Figure 5: The standard deviation of the neutron population calculated by each model when including zero neutron precursor groups for the sub-critical case (a)(b) and the super-critical case (c)(d).

4. Modelling Stochastic Neutron Kinetics with One Group of Delayed Neutron Precursors

It is common to see results for neutron kinetics where one group of delayed neutron precursors have been modelled. Section 4 will serve as a comparison between the different models when one group of delayed neutron precursors are included. These comparisons will demonstrate how the computational execution time of each of model increases as the complexity of the problem increases. Identical temporal discretization and realisation counts have been used for the one delayed neutron precursor group calculations as were used for the zero precursor group calculations.

The same constant reactivity profiles and external neutron source strengths have been used for the simulations in this section. Table 5 shows the simulation time required for each model to produce the relevant results.

4.1. The Survival Probability

The survival probability results including one group of delayed neutron precursor groups are shown in Figure 6. Again, the AMC, PB, FPB models show good agreement in their results. The accuracy of the EEM method does not seem to be affected by the inclusion of one group of delayed neutron precursors. It can be seen that the simulation time has increased slightly for both the AMC and FPB model but not significantly.

4.2. The Extinction Probability

The extinction probability results including one group of delayed neutron precursor groups are shown in Figure 7. As with the results of the zero delayed neutron precursor groups, the AMC model exhibits a natural variation in the results which is clear in Figures 7a and 7c. However, there is still good agreement between the AMC, PB, and FPB models. The inclusion of a delayed neutron precursor group has not appeared to have improved the accuracy of the EEM method. It can, however, be seen that the computation time has increased more sharply for the AMC model than the other models.

The reason that the simulation time of the AMC model has increased significantly, in the calculation of the extinction probability but not the survival probability, is due to the presence of the external neutron source. As the survival probability has been calculated in the absence of the source, if the neutron chain becomes extinct during a particular realisation then the remainder of the realisation does not require computing. This is because in the absence of a source no new neutron will be introduced into the system. The inclusion of delayed neutron precursor groups does not impact the survival probability significantly. Thus, the number of realisations that do not need to be simulated fully stays roughly the same and the impact of the

Table 5: The simulation time (s) for each method to compute the relevant numerical result when modelling one group of delayed neutron precursors. The survival probability simulation times are represented by the columns $S = 0$ as these simulations do not include an external neutron source. All models, excluding the Pál-Bell model, computed the extinction probability, moments, and cumulative distribution results at the same time and are represented by the columns $S = 5$ and $S = 5000$.

	S = 0		**S = 5**		**S = 5000**	
Method	**k = 0.9**	**k = 1.1**	**k = 0.9**	**k = 1.1**	**k = 0.9**	**k = 1.1**
PB	8E-2	8E-2	5E-2	4E-2	4E-2	4E-2
FPB	6E2	6E2	6E2	5E2	7E2	6E2
FGF	/	/	4E-3	3E-3	3E-3	3E-3
AMC	5E2	5E2	4E2	4E2	5E2	5E2
EEM	2E2	2E2	2E2	2E2	2E2	2E2
IEM	/	/	3E2	3E2	2E2	2E2

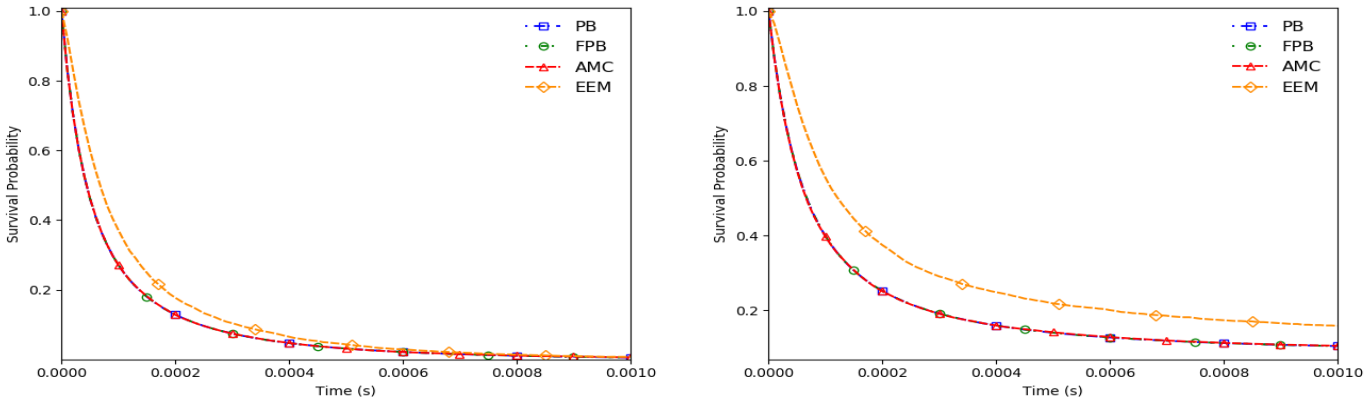

(a) (b)

Figure 6: The survival probability calculated by each model when including one neutron precursor group for the sub-critical case (a) and the super-critical case (b).

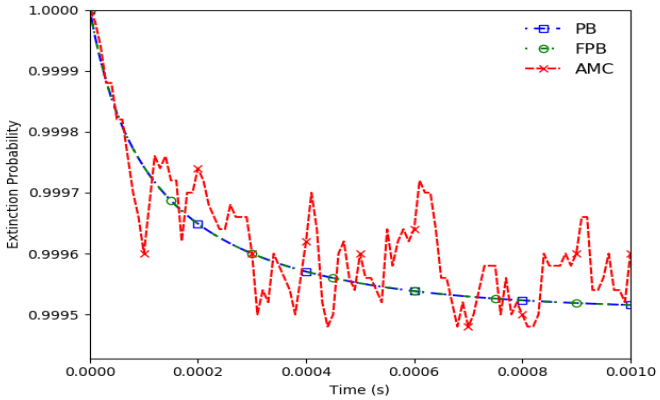

(a) External neutron source: 5 n/s.

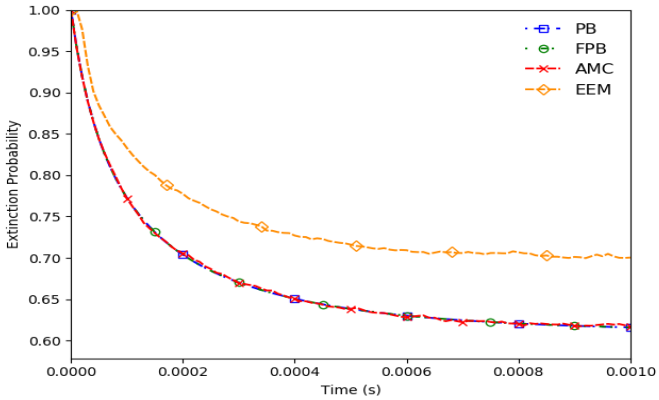

(b) External neutron source: 5000 n/s.

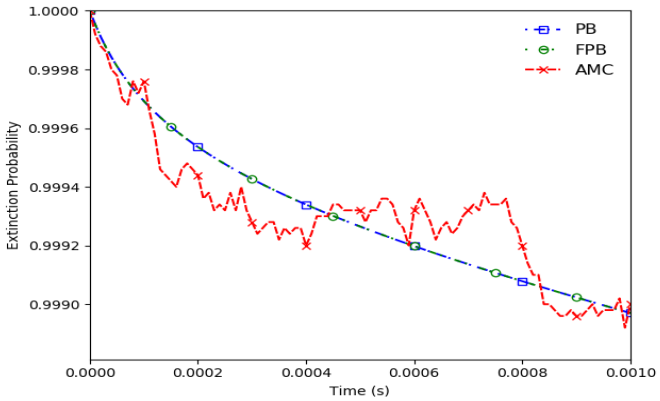

(c) External neutron source: 5 n/s.

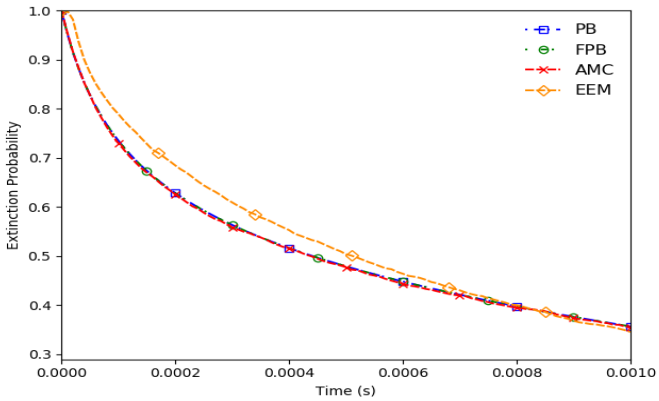

(d) External neutron source: 5000 n/s.

Figure 7: The extinction probability calculated by each model when including one neutron precursor group for the sub-critical case (a)(b) and the super-critical case (c)(d).

extra computations required to model the delayed neutron precursor group is minimised. However, this is only true for the survival probability results as they are the only results that do not include an external neutron source.

4.3. Cumulative Distribution Function (CDF)

The cumulative distribution function results including one group of delayed neutron precursors are shown in Figure 8 and illustrate a similar trend to that seen in Section 3. The computational efficiency of the PB model is far superior to the other three models but are not as accurate when the mean neutron population is low. The EEM method is also less computationally demanding than either the AMC or FPB models but is inaccurate for super-critical systems.

4.4. Population Mean and Variance

The mean and standard deviation of the neutron population when including one group of delayed neutron precursors is shown in Figures 9-10. The inclusion of a delayed neutron precursor group has not appeared to decrease the accuracy of either Itô calculus method compared to that of the zero precursor results. However, the computation time of the FPB model has increased. This can be attributed to the fact that the inclusion of a delayed neutron precursor group significantly increases the computing power required and increases the number of approximations that need to be made when approaching the maximum population of a given entity (prompt population or precursor group population).

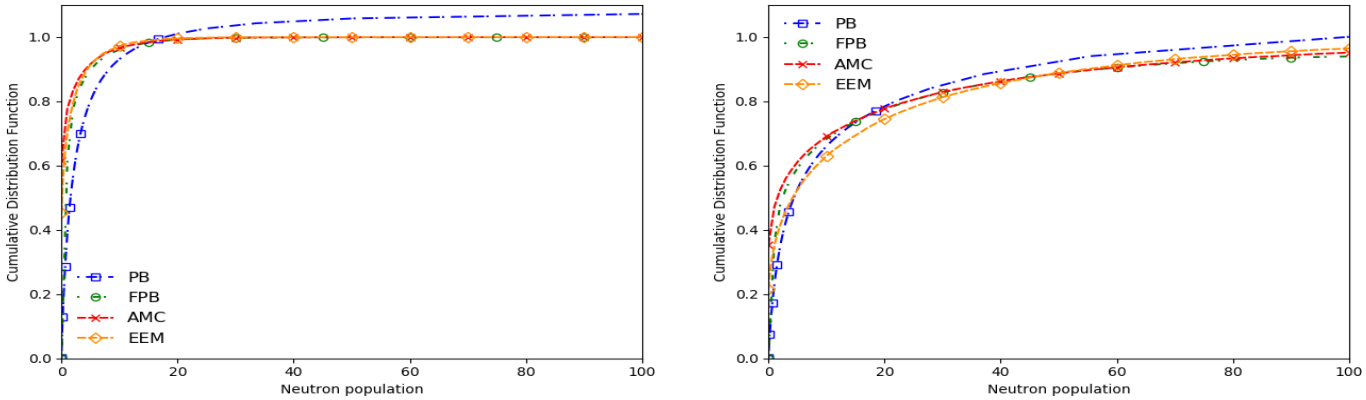

(a) (b)

Figure 8: The cumulative distribution calculated by each model when including one neutron precursor group and an external source strength of 5000 n/s for the sub-critical case (a) and the super-critical case (b). The CDF is computed at time $t = 100$ ms.

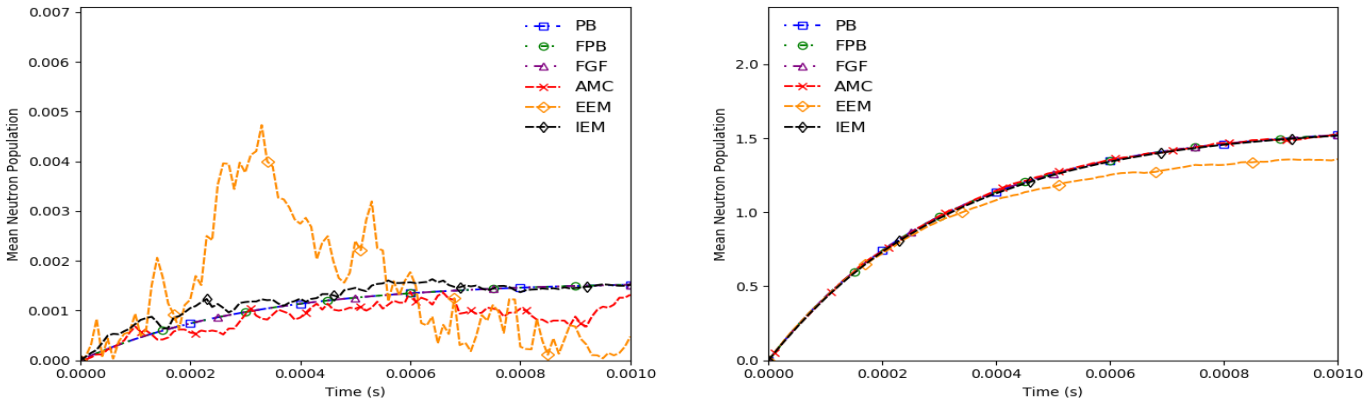

(a) External neutron source: 5 n/s. (b) External neutron source: 5000 n/s.

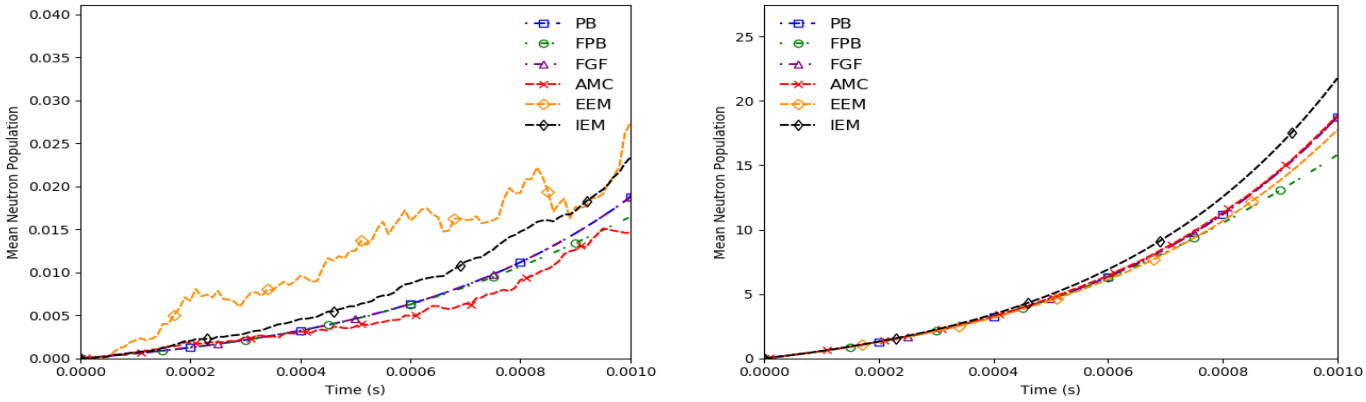

(c) External neutron source: 5 n/s. (d) External neutron source: 5 n/s.

Figure 9: The mean neutron population calculated by each model when including one neutron precursor group for the sub-critical case (a)(b) and the super-critical case (c)(d).

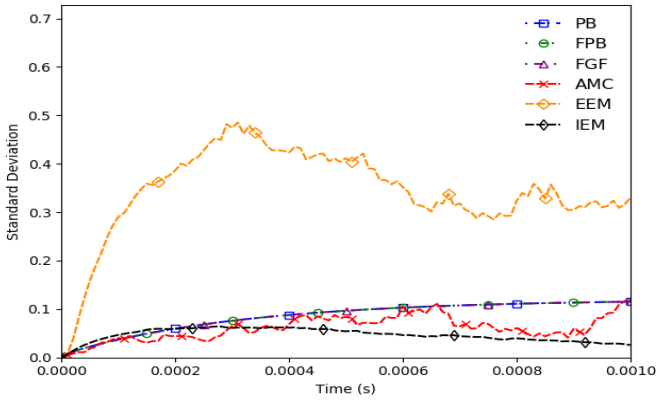

(a) External neutron source: 5 n/s.

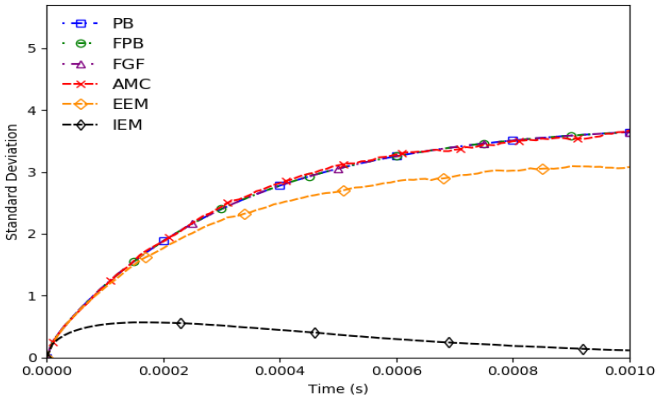

(b) External neutron source: 5000 n/s.

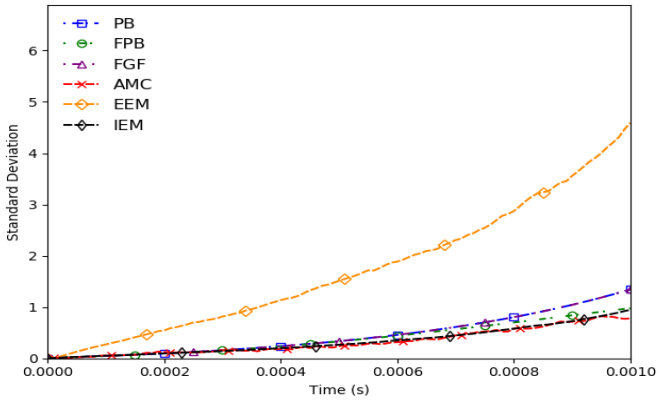

(c) External neutron source: 5 n/s.

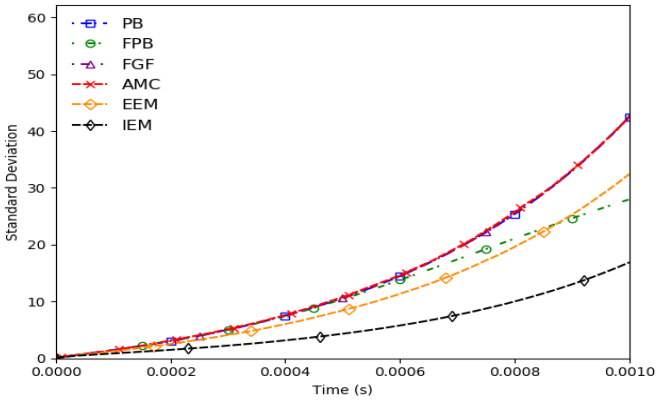

(d) External neutron source: 5000 n/s.

Figure 10: The standard deviation of the neutron population calculated by each model when including one neutron precursor group for the sub-critical case (a)(b) and the super-critical case (c)(d).

5. Modelling Stochastic Neutron Kinetics with Six Groups of Delayed Neutron Precursors

It is most common to include six groups of delayed neutron precursors when modelling neutron kinetics and is essential for evaluating the probability distribution [11]. This section will compare the different computational models in their ability to produce the required numerical results and quantities of interest (QoI) for the the most computational demanding systems involving six delayed neutron precursor groups. These comparisons will highlight the differences in the computational efficiency and numerical accuracy of each of the computational models.

The same constant reactivity profiles and external neutron source strengths have been used for the simulations in this section as in the previous two sections. Table 6 shows the simulation time required for each model to produce the relevant result when including six groups of delayed neutron precursors.

5.1. The Survival Probability

Figure 11 shows the comparison of the models in their ability to compute the survival probability when including six groups of delayed neutron precursors. The FPB model is still showing good agreement with the PB and AMC models. The EEM method is still not showing an agreement with the other three models. As seen in the comparisons that modelled fewer delayed neutron precursor groups, the EEM method decreases in accuracy when the reactivity of the system increases.

5.2. The Extinction Probability

The comparison of the extinction probability when modelling six groups of delayed neutron precursors can be seen in Figure 12. All the models, except the EEM method, are again showing good agreement. As with the previous models that included fewer delayed neutron precursor groups, the AMC results have not converged for the systems with an external neutron source of 5 n/s. However, the results do fluctuate around the results of the PB and FPB models. The EEM method is still not showing good agreement with the other three methods.

5.3. Cumulative Distribution Function (CDF)

The results shown in Figures 13a and 13b show the comparison of the models in their ability to calculate the neutron population distribution when six groups of delayed neutron precursors are included. It is clear that the EEM method shows better agreement with the AMC and FPB models than the PB model for smaller reactivity systems. The same trend is seen, as that shown in Section 4, that the saddle-point method increases in accuracy as the neutron population increases.

5.4. Population Mean and Variance

Figure 14 and Figure 15 show the comparison of all five models computation of the mean and standard deviation of the neutron population respectively. No significant difference in accuracy can be seen in the results of the AMC, FPB, EM, or IEM models compared to their respective results when only modelling one group of delayed neutron precursors. The important thing to note is the times taken for each of the methods to produce their results. The PB and FGF models are 4-5 orders of magnitude more computationally efficient than any of the other models.

Table 6: The simulation time (s) for each method to compute the relevant numerical result when modelling six groups of delayed neutron precursors. The survival probability simulation times are represented by the columns $S = 0$ as these simulations do not include an external neutron source. All models, excluding the Pál-Bell model, computed the extinction probability, moments, and cumulative distribution results at the same time and are represented by the columns $S = 5$ and $S = 5000$.

	S = 0		**S = 5**		**S = 5000**	
Method	**k = 0.9**	**k = 1.1**	**k = 0.9**	**k = 1.1**	**k = 0.9**	**k = 1.1**
PB	1E-1	1E-1	6E-2	6E-2	6E-2	6E-2
FPB	1E4	1E4	1E4	1E4	1E4	1E4
FGF	/	/	3E-3	4E-3	4E-3	3E-3
AMC	1E3	2E3	1E3	1E3	1E3	1E3
EEM	2E2	2E2	2E2	2E2	2E2	2E2
IEM	/	/	3E2	3E2	3E2	3E2

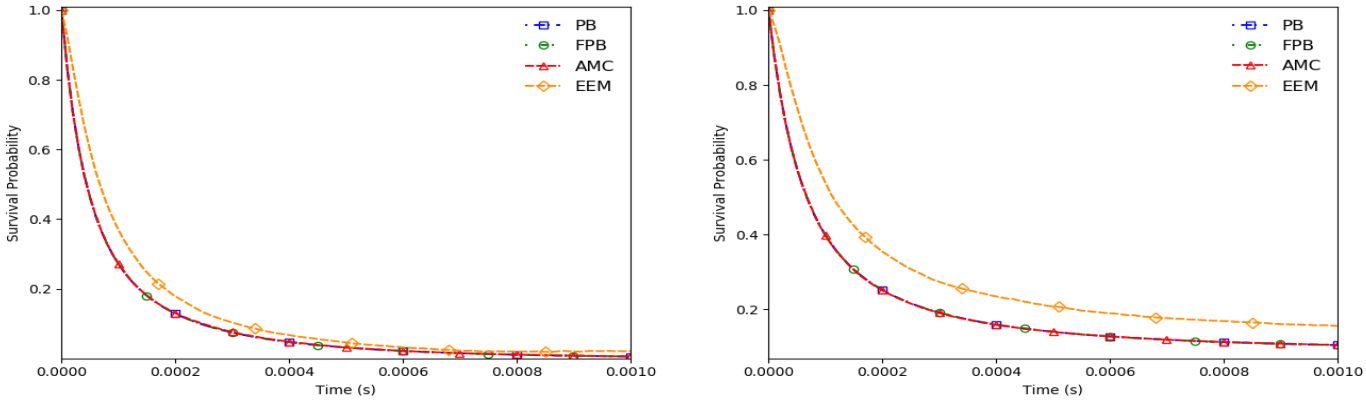

(a) (b)

Figure 11: The survival probability calculated by each model when including six neutron precursor groups for the sub-critical case (a) and the super-critical case (b).

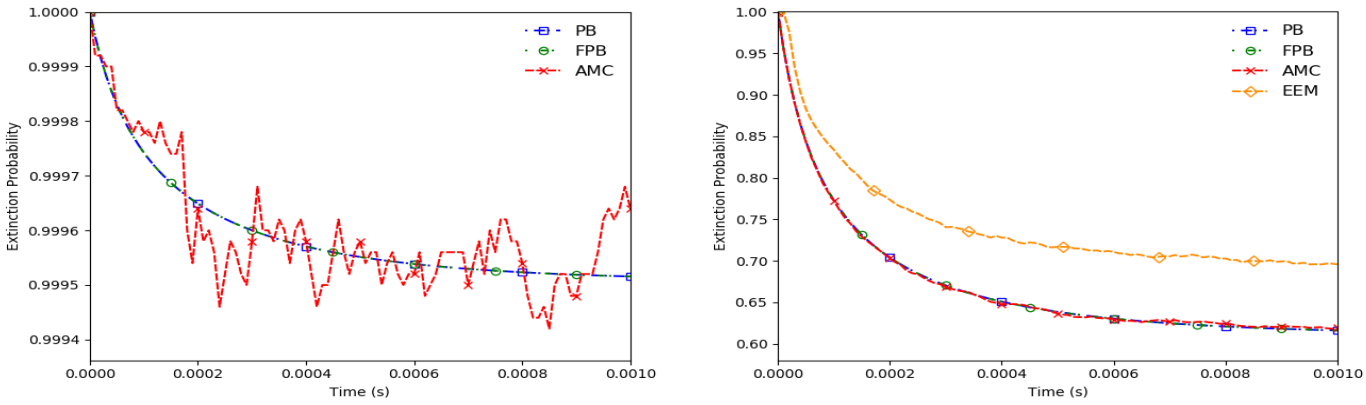

(a) External neutron source: 5 n/s. (b) External neutron source: 5000 n/s.

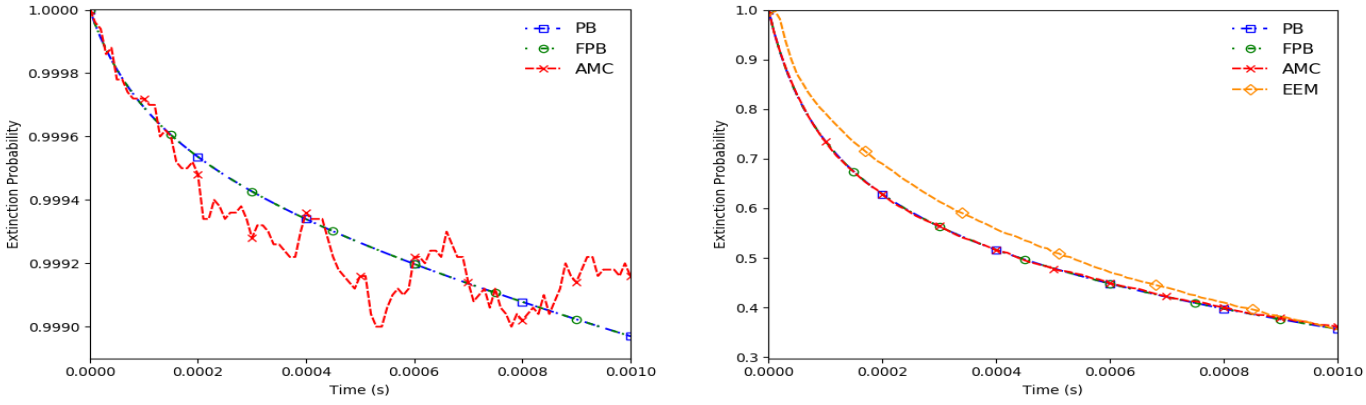

(c) External neutron source: 5 n/s. (d) External neutron source: 5000 n/s.

Figure 12: The extinction probability calculated by each model when including six neutron precursor groups for the sub-critical case (a)(b) and the super-critical case (c)(d).

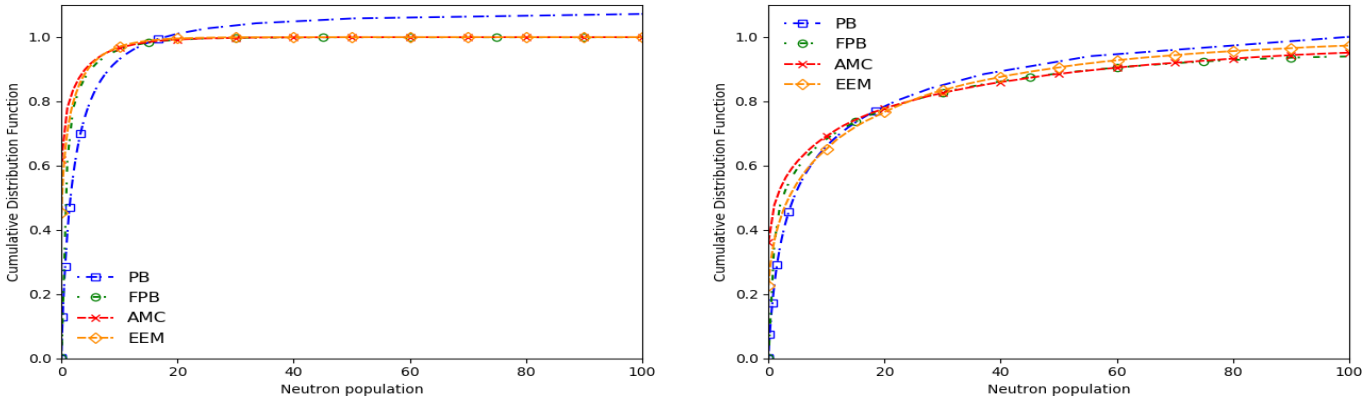

(a) (b)

Figure 13: The cumulative distribution calculated by each model when including six neutron precursor groups and an external source strength of 5000 n/s for the sub-critical case (a) and the super-critical case (b). The CDF is computed at time $t = 100$ ms.

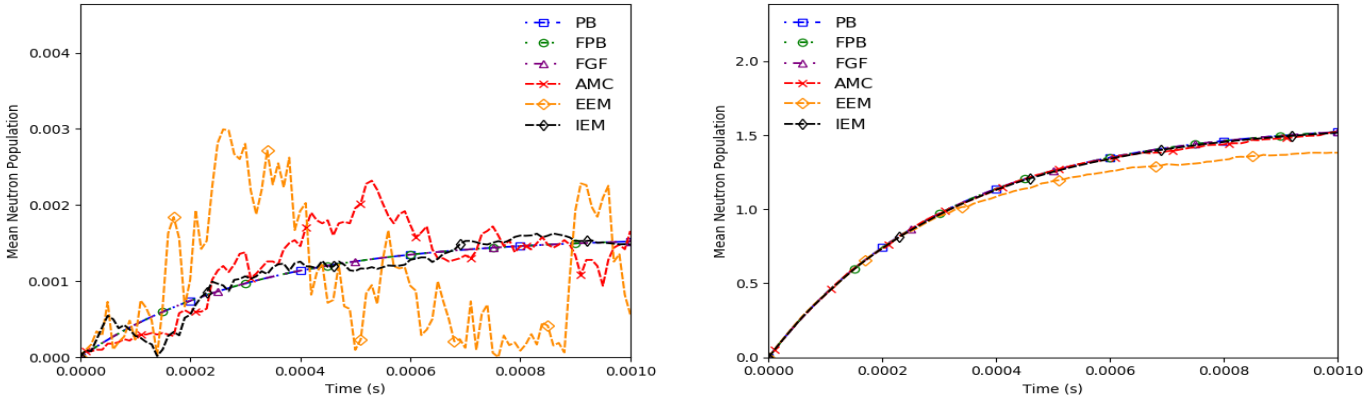

(a) External neutron source: 5 n/s. (b) External neutron source: 5000 n/s.

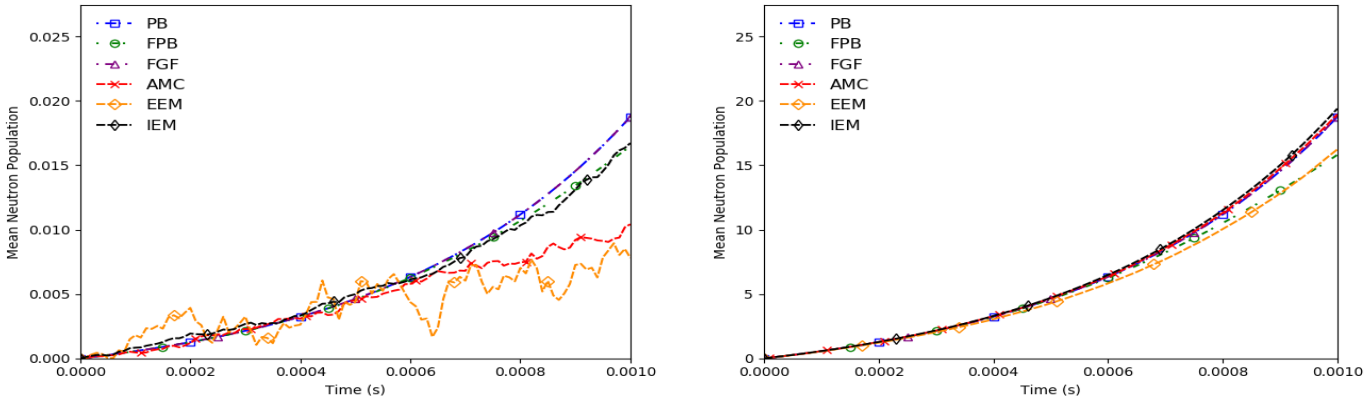

(c) External neutron source: 5 n/s. (d) External neutron source: 5000 n/s.

Figure 14: The mean neutron population calculated by each model when including six neutron precursor groups for the sub-critical case (a)(b) and the super-critical case (c)(d).

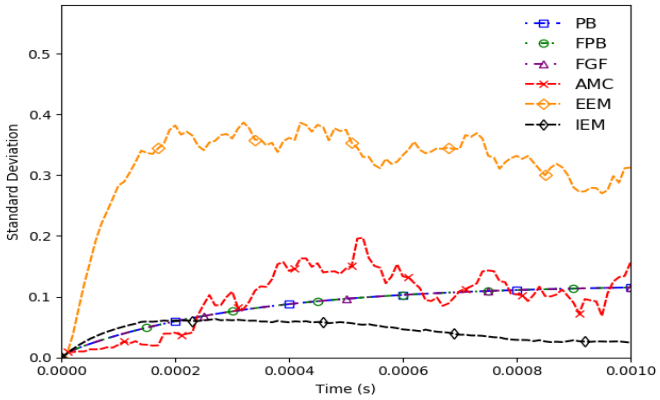

(a) External neutron source: 5 n/s.

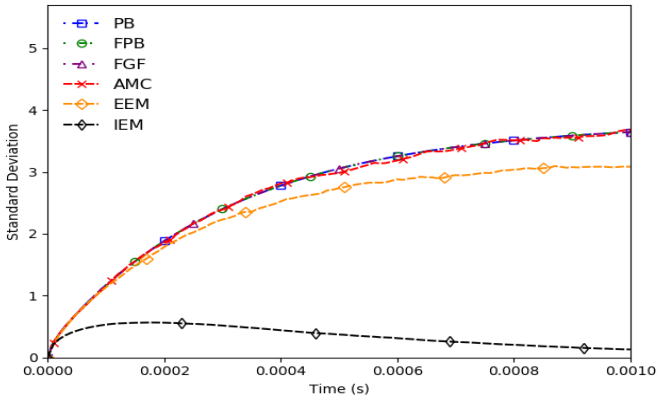

(b) External neutron source: 5000 n/s.

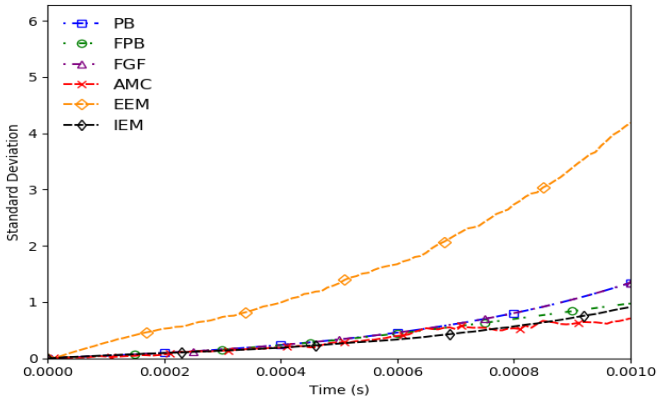

(c) External neutron source: 5 n/s.

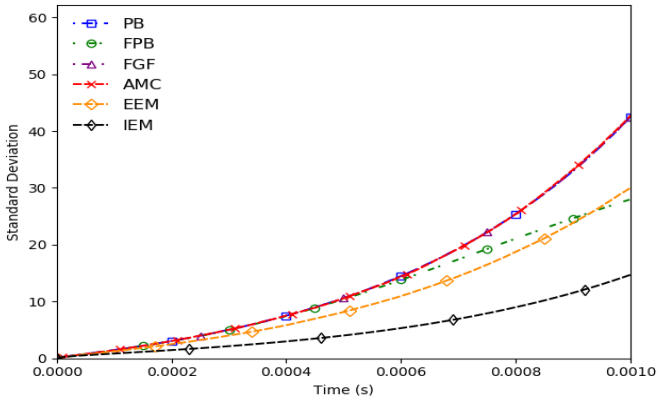

(d) External neutron source: 5000 n/s.

Figure 15: The standard deviation of the neutron population calculated by each model when including six neutron precursor groups for the sub-critical case (a)(b) and the super-critical case (c)(d).

6. Conclusion

In this study, we have developed and implemented five different numerical codes for modelling the stochastic populations of neutrons within low extraneous (external or fixed) neutron source systems. Each numerical code utilised a different set of mathematical and computational models. These mathematical and computational models were: the analog Monte-Carlo (AMC), the forward probability balance equations (FPB), the generating function form of the forward probability balance equations (FGF), the generating function form of the backward probability balance equation or Pál-Bell (PB), and an Itô calculus model utilising explicit (EEM) and implicit (IEM) Euler-Maruyama discretization. Each computational model has been used to generate various numerical results and quantities of interest (QoI) which were used to compare and contrast the numerical accuracy and computational efficiency of the models against one another. The numerical results and QoI chosen for the comparisons were: the survival probability, the extinction probability, the mean and standard deviation in the neutron population, and the cumulative distribution function of the neutron population.

From the results presented in Sections 3-5, it is clear that the PB model was the most computationally efficient and numerically accurate model when simulating low neutron source systems.

The computational efficiency requirement is an important feature of the numerical models. This is especially important if the computational models are extended to include energy [32] and spatial dependence [12, 33]. In these cases the simulation time will become critically important to the viability of the computational method [34, 35]. It is also important to note that the survival probability, extinction probability, mean, and standard deviation results were directly extracted from the equations of the mathematical model and that no approximations where required when calculating the numerical results. It is also possible to directly extract higher order moments such as skewness and kurtosis from the PB model. It was also demonstrated that the accuracy of the saddle-point equations decrease for very small values of n_{prob} which is consistent with the work of Williams [11, 12].

The results also highlight that although the AMC and FPB model produce accurate results for very low neutron populations they are both computationally less efficient in comparison to the PB model.

It has also been shown, in this study, that the numerical accuracy of the FPB model starts to decrease significantly when required to accurately model larger neutron populations. This issue is more acute when modelling delayed neutron precursor groups as the number of ODEs that need to be solved increases and thus the maximum prompt neutrons that can be modelled must be decreased.

The FGF model has been used as a form of verification for the other methods while generating the mean and standard deviation results. The computation efficiency of FGF model when computing the moments was found to be even greater than the PB model. However, as discussed in Appendix D the extension of the model to include energy and spatial dependence results in complex numerical difficulties which the PB model avoids.

It has been shown that while certain simulations are capable of being modelled by an Itô calculus approach, the model is unsuited for very low neutron populations. It was found that the method (regardless of discretization scheme) is much better suited for sub-critical systems than super-critical. The method has been used to replicate certain results from the literature (Appendix H). However, the scenarios in Appendix H have a larger expected neutron population than the scenarios presented in this study. It appears that the method is incapable of accurately modelling such low numbers of neutrons. The results of the method are dependent upon the temporal discretization, with respect to the nuclear and neutron kinetics data being used, and as such careful consideration to all parameters used is required when constructing such a model.

Data Statement

In accordance with EPSRC funding requirements all supporting data used to create figures in this paper may be accessed at the following URL: https://doi.org/10.5281/zenodo.4419858.

CRediT authorship contribution statement

T.L. Gordon: Conceptualization, Methodology, Software, Data curation, Formal analysis, Writing - original draft, Writing - review editing, Visualization, Investigation. **C.C. Cooling:** Conceptualization, Methodology, Writing - review editing. **M.M.R. Williams:** Conceptualization, Methodology, Writing - review editing. **M.D. Eaton:** Conceptualization, Methodology, Funding acquisition, Writing - review editing.

Declaration of Competing Interest

The authors declare that they have no known competing financial interests or personal relationships that could have appeared to influence the work reported in this paper.

Acknowledgements

Mr T.L. Gordon would like to acknowledge the support of Engineering and Physical Sciences Research Council (EPSRC) through the Doctoral Training Partnership (DTP) PhD scheme (EPSRC Grant number: EP/R513052/1). Mr T.L. Gordon also acknowledges the industrial and financial support of Rolls-Royce. Dr M.D. Eaton and Dr C.M. Cooling would like to thank EPSRC for their support through the following grants: Adaptive Hierarchical Radiation Transport Methods to Meet Future Challenges in Reactor Physics (EPSRC grant number: EP/J002011/1) and Nuclear Reactor Kinetics Modelling and Simulation Tools for Small Modular Reactor (SMR) Start-up Dynamics and Nuclear Critically Safety Assessment of Nuclear Fuel Processing Facilities (EPSRC grant number: EP/K503733/1). The authors wish to thank Professor Thomas Sutton (adjunct Professor in the department of mechanical, aerospace and nuclear engineering, Rensselaer Polytechnic Institute, Troy, New York, USA) for his invaluable advice on stochastic neutron kinetics. Finally, the authors would also like to thank the high performance computing (HPC) service support team at Imperial College London led by research service computing manager Mr M. Harvey.

Appendix A. Test Cases

A system with an extraneous neutron source of 5 n/s and one with an extraneous neutron source of 5000 n/s are compared in this study. The nuclear and neutron kinetics data of both systems are identical and are presented in Table 7.

Table 7: The variables used to define the data used in the example test case when modelling zero, one, and six groups of delayed neutron precursors.

Variables	Zero Groups	One Group	Six Groups
Σ_f	5.0	5.0	5.0
$\Sigma_{a,k=0.9}$	13.391779	13.483644	13.483644
$\Sigma_{a,k=1.1}$	10.956911	11.032072	11.032072
ν	2200.0	2200.0	2200.0
$P_{f,0}$	0.0319004	0.0319004	0.0319004
$P_{f,1}$	0.1725213	0.1725213	0.1725213
$P_{f,2}$	0.3361397	0.3361397	0.3361397
$P_{f,3}$	0.3038798	0.3038798	0.3038798
$P_{f,4}$	0.1266155	0.1266155	0.1266155
$P_{f,5}$	0.0261843	0.0261843	0.0261843
$P_{f,6}$	0.0026170	0.0026170	0.0026170
$P_{f,7}$	0.0001421	0.0001421	0.0001421
β	/	0.00681	0.00681
β_1	/	0.00681	0.000210
β_2	/	/	0.001134
β_3	/	/	0.001107
β_4	/	/	0.003154
β_5	/	/	0.000901
β_6	/	/	0.000307
λ_1	/	0.73919	0.01249
λ_2	/	/	0.03182
λ_3	/	/	0.10938
λ_4	/	/	0.31699
λ_5	/	/	1.3598
λ_6	/	/	8.63638

Appendix B. Forward Probability Balance Deviations at Large Populations

The results in Sections 3-5 illustrate the limitations of the FPB model when simulating large numbers of neutrons. The results start to significantly deviate from the true solution when the probability $P(n > n_{max})$ that the neutron population is greater than n_{mat} starts to increase and the approximation used at $n = n_{max}$ is required. Figure 16 illustrates this concept.

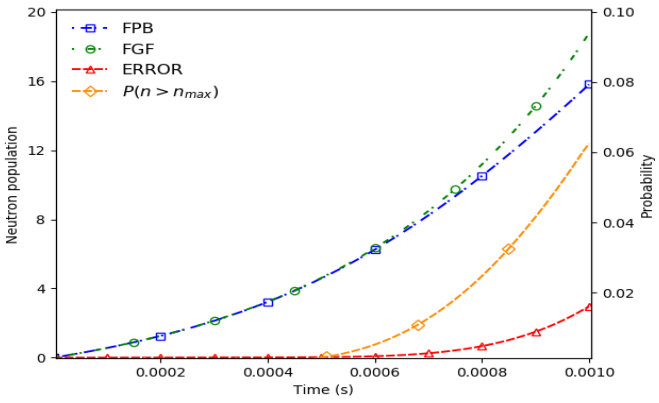

Figure 16: The deviation of the FPB model from the FGF model while simulating the mean neutron population for $k_{eff} = 1.1$ and $S = 5000\,\text{n/s}$ including six groups of delayed neutron precursors. The probability $P(n > n_{max})$ is also shown.

Appendix C. Derivation of the Moment Equations of the Generating Function Form of the Forward Probability Balance Equations

The generating function form of the forward probability balance equation for a point model may be written as [17]:

$$\frac{\partial F(x,\vec{y},t)}{\partial t} = g(x,\vec{y},t)\frac{\partial F(x,\vec{y},t)}{\partial x} + \sum_{m=1}^{M}\lambda_m(x-y_m)\frac{\partial F(x,\vec{y},t)}{\partial y_m} + S(t)(x-1)F(x,\vec{y},t) \tag{C.1}$$

where

$$g(x,\vec{y},t) = \lambda_c(t)(1-x) + \lambda_f(t)(f(x,\vec{y})-x) \tag{C.2}$$

$$f(x,\vec{y}) = \left(1-\bar{\nu}(1-\beta)(1-x)+\frac{1}{2}\hat{\chi}_2(1-x)^2+\cdots\right)\prod_{m=1}^{M}(1-\bar{\nu}\beta_m(1-y_m)) \tag{C.3}$$

$$\hat{\chi}_2 = \sum_{\nu=2}^{\nu_{\max}}\frac{\nu!}{(\nu-2)!}p_\nu \tag{C.4}$$

where p_ν is the probability that ν neutrons are emitted in a fission event.

It is now possible to define the following moments associated with (Eq. C.1):

$$\left.\frac{\partial F(x,\vec{y},t)}{\partial x}\right|_{x=\vec{y_m}=1} = \left.\sum_{n=0}^{\infty}\sum_{c_m=0}^{\infty} n x^{n-1} y_m^{c_m} p(n,...,t)\right|_{x=\vec{y_m}=1} = \langle N\rangle = \bar{N} \tag{C.5}$$

$$\left.\frac{\partial F(x,\vec{y},t)}{\partial y_m}\right|_{x=\vec{y_m}=1} = \left.\sum_{n=0}^{\infty}\sum_{c_m=0}^{\infty} x^n c_m y_m^{c_m-1} p(n,...,t)\right|_{x=\vec{y_m}=1} = \langle C-i\rangle = \bar{C}_i \tag{C.6}$$

$$\left.\frac{\partial^2 F(x,\vec{y},t)}{\partial x\partial y_m}\right|_{x=\vec{y_m}=1} = \left.\sum_{n=0}^{\infty}\sum_{c_m=0}^{\infty} n x^{n-1} c_m y_m^{c_m-1} p(n,...,t)\right|_{x=\vec{y_m}=1} = \langle N c_m\rangle = \mu_{Ni} \tag{C.7}$$

$$\left.\frac{\partial^2 F(x,\vec{y},t)}{\partial x^2}\right|_{x=\vec{y_m}=1} = \left.\sum_{n=0}^{\infty}\sum_{c_m=0}^{\infty} n(n-1) x^{n-2} y_m^{c_m} p(n,...,t)\right|_{x=\vec{y_m}=1} = \langle N(N-1)\rangle = \mu_{NN} \tag{C.8}$$

$$\left.\frac{\partial^2 F(x,\vec{y},t)}{\partial y_m\partial y_j}\right|_{x=\vec{y_m}=1} = \left.\sum_{n=0}^{\infty}\sum_{c_m=0}^{\infty} x^n c_m c_j y_m^{c_m-1} y_j^{c_j-1} p(n,...,t)\right|_{x=\vec{y_m}=1} = \langle c_m C_j\rangle = \mu_{ij} \tag{C.9}$$

(Eqs. 18-23) are then obtained after differentiating (Eq. C.1) with respect to the corresponding variable. The following differentials will be demonstrated for one group of delayed neutron precursors for simplicity:

$$\left.\frac{\partial g(x,y)}{\partial x}\right|_{x=y=1} = \left.-\lambda_c-\lambda_f+\lambda_f f_x(x,y)\right|_{x=y=1} = \lambda_f\bar{\nu}(1-\beta)-\lambda_a \tag{C.10}$$

$$\left.\frac{\partial^2 g(x,y)}{\partial x^2}\right|_{x=y=1} = \lambda_f f_{xx}(x,y)\Big|_{x=y=1} = \hat{\chi}_2 \tag{C.11}$$

$$\left.\frac{\partial g(x,y)}{\partial y}\right|_{x=y=1} = \lambda_f f_y(x,y)\Big|_{x=y=1} = \bar{\nu}\beta\lambda_f \tag{C.12}$$

$$\left.\frac{\partial^2 g(x,y)}{\partial x\partial y}\right|_{x=y=1} = \lambda_f f_{xy}(x,y)\Big|_{x=y=1} = \lambda_f\bar{\nu}(1-\beta)\bar{\nu}\beta \tag{C.13}$$

Appendix D. Hurwitz, MacMillan Equations Including one Delayed Neutron Group

It is useful to include the forward form of the generating function equation, as solved numerically by Hurwitz et al [36], and its associated moments as follows. This will highlight the additional numerical difficulties in the forward form compared with those of the backward form.

The traditional equation for the forward generating function is

$$\frac{\partial F(x,\vec{y},t)}{\partial t} = g(x,\vec{y},t)\frac{\partial F(x,\vec{y},t)}{\partial x} + \sum_{m=1}^{M}\lambda_m(x-y_m)\frac{\partial F(x,\vec{y},t)}{\partial y_m} + S(x-1)F(x,\vec{y},t) \tag{D.1}$$

with the initial condition $F(x,\vec{y},t) = 1$. If we re-write this equation in the more compact notation for one group of delayed neutron precursors:

$$\frac{\partial F(x,y,t)}{\partial t} + \frac{dx}{dt}\frac{\partial F(x,y,t)}{\partial x} + \frac{dy}{dt}\frac{\partial F(x,y,t)}{\partial y} \equiv \frac{DF(x,y,t)}{Dt} = S(x-1)F(x,y,t) \tag{D.2}$$

with

$$\frac{dx}{dt} = -g(x,y,t),\ \frac{dy}{dt} = -\lambda(x-y),\ \frac{dF}{dt} = S(x-1)F \tag{D.3}$$

then we may write the equations for the moments required in the saddle-point equations as

$$\frac{DF_x}{Dt} = [g_x + S(x-1)]F_x + \lambda F_y + SF \tag{D.4}$$

$$\frac{DF_{xx}}{Dt} = [2g_x + S(x-1)]F_{xx} + 2\lambda F_{xy} + (g_{xx}+2S)F_x \tag{D.5}$$

$$\frac{DF_y}{Dt} = [g_y + S(x-1)]F_x + (S(x-1)-\lambda)F_y \tag{D.6}$$

$$\frac{DF_{yy}}{Dt} = [2g_y + S(x-1)]F_{xy} + g_{yy}F_x + (S(x-1)-2\lambda)F_{yy} \tag{D.7}$$

$$\frac{DF_{xy}}{Dt} = [g_x + S(x-1) - \lambda]F_{xy} + \lambda F_{yy} + (g_{xy}+S)F_x + (g_y + S(x-1))F_{xx} + SF_y \tag{D.8}$$

As explained by Williams and Eaton [11, 12] the main challenge is the numerical evaluation of the total derivative term $\frac{DF(x,y,t)}{Dt}$ and is the point at which the advantages of the backward formalism enter. With the backward method we need only solve a set of first order, coupled, non-linear differential equations and in addition there is the advantage of including energy and space dependence in a straightforward way. The forward form, as illustrated above, is not simple to solve numerically as a reading of the Hurwitz papers [36] will indicate and, moreover, to include space and energy described by Stacey [37] complicates the total derivative D/Dt even more. Inclusion of more groups of delayed neutrons also adds additional terms to D/Dt.

Appendix E. The Gamma Distribution Approximation

Harris [38] illustrated in highly multiplicative systems, the distribution will tend to the gamma distribution. The gamma probability density function may be written as:

$$P(n,t) = \frac{\eta(t)}{\bar{n}(t)\Gamma(\eta(t))}\left(\frac{\eta(t)n}{\bar{n}(t)}\right)^{\eta(t)-1}\exp\left(-\frac{\eta(t)n}{\bar{n}(t)}\right) \tag{E.1}$$

where $\eta(t) = \bar{n}^2(t)/\sigma_N^2(t)$. Both $\bar{n}$ and σ_N can be calculated with the FGF model explained in Section 2.3.

Figure 17 shows an example of the CDF generated using the gamma approximation compared to the other models described in this study. As shown in Figure 17 the gamma approximation shows good agreement with the other models in this study. A significant portion of the gamma distribution matches the AMC and FPB distributions. The approximation is an effective method for very accurately calculating the most prominent region of the CDF. However, it should be noted that the applicability of this method to low external neutron source problems is limited due to the known deviation from the true solution at the tails of the distribution [11, 12].

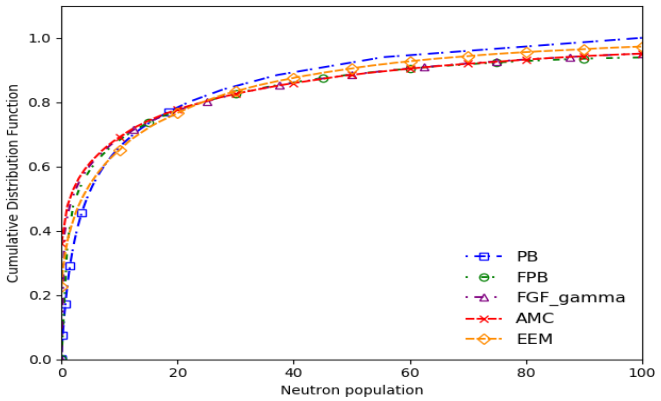

Figure 17: The cumulative distribution calculated by each model (including the gamma approximation) when including six neutron precursor groups and an external source strength of 5000 n/s for the super-critical case. The CDF is computed at time $t = 100$ ms.

Appendix F. The Relationship between the Exact Probability Balance Method and Fokker-Plank (Itô) Method for Neutron Fluctuations

The traditional forward and backward forms of the probability balance equations for the neutron populations are well-developed and can deal with a variety of practical problems [11, 12, 13]. Complementary to these methods is that based on the Langevin technique in which the deterministic form of the problem are defined and random source terms added to stimulate the solution. The form these noise sources take have been subject of investigation for many years. Recently a variant of the Langevin method has been proposed by Allen [39] who relates it to a type of stochastic differential equation (SDE) known as Itô equations. We will consider a simple example, namely the classic birth and death problem to compare the exact method (probability balance) with the Itô results which in turn are related to the Fokker-Plank equation. As a measure of comparison we choose the extinction problem which calculates the probability that at a given time the number of neutrons becomes zero.

The Forward generating equation for the one speed point model is with no delayed neutrons:

$$F(x,t) = \sum_{n=0}^{\infty} x^n P(n,t) \tag{F.1}$$

$$\frac{\partial F(x,t)}{\partial t} = \left[\lambda_f(f(x) - x) + \lambda_c(1-x)\right]\frac{\partial F(x,t)}{\partial x} \tag{F.2}$$

where $\lambda_c = \nu\Sigma_c$, $f(x) = \sum_{n=0}^{\infty} x^n p(n)$, and $p(n)$ being the probability that n neutrons are emitted in a fission event. The initial condition is $F(x,0) = x$, *i.e.* $P(n,0) = \delta_{n,1}$.

The backward equation for $F(x,t)$ is:

$$-\frac{\partial F(x,t|s)}{\partial s} = \lambda_c - (\lambda_c + \lambda_f)F(x,t|s) + \lambda_f f(F(x,t|s)) \tag{F.3}$$

In this case:

$$F(x,t|s) = \sum_{n=0}^{\infty} x^n P(n,t|s) \tag{F.4}$$

where $P(n,t|s)$ is the probability that if one neutron is injected at time s there will be n neutrons at time t. Because the transition coefficients, λ, are independant of time, we may write $t - s \to t$ and (Eq. F.3) becomes:

$$\frac{\partial F(x,t)}{\partial t} = \lambda_c - (\lambda_c + \lambda_f)F(x,t) + \lambda_f f(F(x,t)) \tag{F.5}$$

Let us note from the definition of the generating function that if we set $x = 0$ we find $F(0,t) = P(0,t)$. Similarly if we differentiate F with respect to x and set $x = 0$ we find $F'(0,t) = P(1,t)$, etc. We may also see that:

$$\frac{\partial F(x,t)}{\partial x} = \sum_{n=0}^{\infty} n x^{n-1} P(n,t) \tag{F.6}$$

Then if $x = 1$:

$$\left.\frac{\partial F}{\partial x}\right|_{x=1} = \sum_{n=0}^{\infty} nP(n,t) = \langle n(t)\rangle \tag{F.7}$$

Similarly,

$$\frac{\partial^2 F(x,t)}{\partial x^2} = \sum_{n=0}^{\infty} n(n-1)x^{n-2}P(n,t); \tag{F.8}$$

then if $x = 1$,

$$\left.\frac{\partial^2 F}{\partial x^2}\right|_{x=1} = \sum_{n=0}^{\infty} n(n-1)P(n,t) = \langle n(t)^2\rangle - \langle n(t)\rangle; \tag{F.9}$$

From which we may obtain the variance $\sigma_{\mathrm{n}}^2(t) = \langle n(t)^2\rangle - \langle n(t)\rangle^2$.

From the backward equation we find by differentiation with respect to x :

$$\begin{aligned}\frac{\partial F'}{\partial t} &= -(\lambda_f + \lambda_c)F' + \lambda_f \frac{d}{dx} f(F) \\ &= -(\lambda_f + \lambda_c)F' + \lambda_f F' \frac{d}{dF} f(F)\end{aligned} \tag{F.10}$$

Setting $x = 1$ and observing that:

$$\frac{d}{dF} f(F) = \sum_{n=0}^{\infty} nF^{n-1}p(n) \tag{F.11}$$

for $F = 1$ this becomes $\frac{d}{dF} f(F)|_{F=1} = \sum_{n=0}^{\infty} np(n) = \bar{\nu}$ which is the mean number of neutrons per fission. The equation for the mean is then:

$$\frac{d\langle n(t)\rangle}{dt} = (\bar{\nu}\lambda_f - \lambda_a)\langle n(t)\rangle \tag{F.12}$$

where $\lambda_a = \lambda_f + \lambda_c$.

If we now differentiate the generating function once more with respect to x we find

$$\begin{aligned}\frac{\partial F''}{dt} &= -(\lambda_f + \lambda_c)F'' + \lambda_f \frac{d}{dx}\left(F' \frac{d}{dF} f(F)\right) \\ &= -(\lambda_f + \lambda_c)F'' + \lambda_f \left(F'' \frac{d}{dF} f(F) + (F')^2 \frac{d^2}{dF^2} f(F)\right)\end{aligned} \tag{F.13}$$

Setting $F = 1$ leads, with $F''(1,t) = \mu(t)$, to

$$\frac{d\mu(t)}{dt} = (\bar{\nu}\lambda_f - \lambda_a)\mu(t) + \langle \nu(\nu-1)\rangle \lambda_f \langle n(t)\rangle^2 \tag{F.14}$$

with $\langle \nu(\nu-1)\rangle = \sum_{n=0}^{\infty} n(n-1)p(n)$, which is related to the variance of the number of neutrons emitted per fission. Thus we have equations for the mean and the variance of the neutron number density.

Let us now derive similar equations using the forward generating function. The equation for the mean is the same as before,

$$\frac{d\langle n(t)\rangle}{dt} = (\bar{\nu}\lambda_f - \lambda_a)\langle n(t)\rangle \tag{F.15}$$

But that for $\mu(t)$ is

$$\frac{d\mu(t)}{dt} = 2(\bar{\lambda}_f - \lambda_a)\mu(t) + \lambda_f \langle \nu(\nu-1)\rangle \langle n(t)\rangle \tag{F.16}$$

which looks very different from the backward equation (Eq. F.14). If we set $\alpha = \bar{\nu}\lambda_f - \lambda_a$, we have $\langle n(t)\rangle = \exp\{\alpha t\}$. The solution for $\mu(t)$ from both equations gives

$$\mu(t) = \frac{\lambda_f}{\alpha}\langle \nu(\nu-1)\rangle e^{\alpha t}(e^{\alpha t} - 1) \tag{F.17}$$

It is convenient to write equation(F.14) in terms of the variance to get

$$\frac{d\sigma^2}{dt} = 2\alpha\sigma^2 + [\langle \nu(\nu-1)\rangle \lambda_f - \bar{\nu}\lambda_f + \lambda_f + \lambda_c]\langle n\rangle \tag{F.18}$$

The square bracket may also be written as

$$\sigma_{VV}^2 = \left[\langle (\nu-1)^2\rangle \lambda_f + \lambda_c\right]\langle n\rangle = \beta\langle n\rangle, \tag{F.19}$$

where β must not be mistaken for the delayed neutron fraction. Allen [39] and Dalfes [40] show this to be the variance of the fission terms. Dalfes also shows that we can write the Fokker Planck equation for the probability distribution as

$$\frac{\partial P(n,t)}{\partial t} = -\alpha \frac{\partial}{\partial n}(nP(n,t)) + \frac{1}{2}\beta \frac{\partial^2}{\partial n^2}(nP(n,t)) \tag{F.20}$$

where $P(n,0) = 1$. The Itô equation associated with the above Fokker-Planck equation is

$$dX(t) = \alpha X(t)dt + \sqrt{\beta X(T)}dW(t) \tag{F.21}$$

with $X(0) = 1$. (Eq. (F.21) can be used for simulation purposes. (Eq. F.20) has the solution

$$P(n,t) = \frac{2\alpha}{\beta(e^{\alpha t} - 1)}\left(\frac{e^{\alpha t}}{n}\right)^{1/2} \exp\left(-\frac{2\alpha(e^{\alpha t} + n)}{\beta(e^{\alpha t} - 1)}\right) I_1\left(\frac{4\alpha(ne^{\alpha t})^{1/2}}{\beta(e^{\alpha t} - 1)}\right) \tag{F.22}$$

where $I_1(x)$ is the modified Bessel function. Now from this we may verify that the mean and the variance are

$$\langle n(t)\rangle = e^{\alpha t} \qquad \sigma^2(t) = \frac{\beta}{\alpha} e^{\alpha t}(e^{\alpha t} - 1) \tag{F.23}$$

The extinction probability cannot be obtained from P(0,t) in (Eq. F.22) but we can calculate the total number of neutrons surviving after time t from

$$S(t) = \int_0^{\infty} dnP(n,t) = 1 - \exp\left(-\frac{2\alpha e^{\alpha t}}{\beta(e^{\alpha t} - 1)}\right). \tag{F.24}$$

From which the extinction probability $E(t)$ is given by (in the Fokker Planck approximation)

$$E(t) = 1 - S(t) = \exp\left(-\frac{2\alpha e^{\alpha t}}{\beta(e^{\alpha t} - 1)}\right) \tag{F.25}$$

We may also calculate the exact value of the extinction probability from the generating functions (Eq. F.2) or (Eq. F.3). If we take the backward equation we see that we need

$$\frac{\partial E(t)}{\partial t} = \lambda_c - (\lambda_c + \lambda_f)E(t) + \lambda_f f(E(t)) \tag{F.26}$$

subject to $E(0) = 1$. This is easily done numerically but by making an assumption we may do it analytically. Thus we assume the simple birth death problem in which two neutrons are emitted per fission, *i.e.* $p(n) = \delta_{n,2}$ or $f(x) = x^2$. We may then write (Eq. F.26) as

$$\frac{dE}{dt} = (1 - E)(\lambda_c - \lambda_f E) \tag{F.27}$$

This equation is readily solved to give

$$E(t) = \frac{\lambda_c(e^{(\lambda_f - \lambda_c)t} - 1)}{\lambda_f e^{(\lambda_f - \lambda_c)t} - \lambda_c} \tag{F.28}$$

This is to be compared with the Fokker Plank result of (Eq. F.25) with $p(n) = \delta_{n,2}$ and leads to

$$E_{FP}(t) = \exp\left(-\frac{2(\lambda_f - \lambda_c)e^{(\lambda_f - \lambda_c)t}}{(\lambda_f + \lambda_c)(e^{(\lambda_f - \lambda_c)t} - 1)}\right) \tag{F.29}$$

Thus we must compare (Eq. F.28) and (Eq. F.29). We note that in both cases that if $\lambda_f \leq \lambda_c$, *i.e.* sub-critical, the extinction probability goes to unity; extinction is certain. On the other hand, if $t \to \infty$, we find

$$E(\infty) = \frac{\lambda_c}{\lambda_f} \qquad \text{and} \qquad E_{FP}(\infty) = \exp\left(-\frac{2(\lambda_f - \lambda_c)}{(\lambda_f + \lambda_c)}\right) \tag{F.30}$$

If in the Fokker-Plank case we write $\lambda_f = \lambda_c + \epsilon$ and expand to order ϵ

$$E_{FP}(\infty) = \exp\left(-\frac{(\lambda_f - \lambda_c)}{\lambda_f}\right) \approx 1 - \frac{(\lambda_f - \lambda_c)}{\lambda_f} = \frac{\lambda_c}{\lambda_f} \tag{F.31}$$

That means that in the limit when λ_c is close to λ_f the results are similar. Clearly this indicated that the Fokker-Plank and, by association, the Itô method are only valid for large extinction probabilities.

Let us re-write (Eq. F.28) and (Eq. F.29) by defining $r = \lambda_c/\lambda_f$ and $\tau = \lambda_f t$, then we have

$$E(\tau) = \frac{r(e^{(1-r)\tau} - 1)}{e^{(1-r)\tau} - r} \qquad \text{and} \qquad E_{FP}(\tau) = \exp\left(-\frac{2(1-r)e^{(1-r)\tau}}{(1+r)(e^{(1-r)\tau} - 1)}\right) \tag{F.32}$$

Numerical values of these expressions are shown in Figure 18 for a range of r values. Clearly, as r approaches unity, the two expressions become closer; physically this means when the system is only very slightly super-critical. For high super-criticality the error is significant. These results suggest that for neutronic problems the Itô calculus is not necessarily adequate.

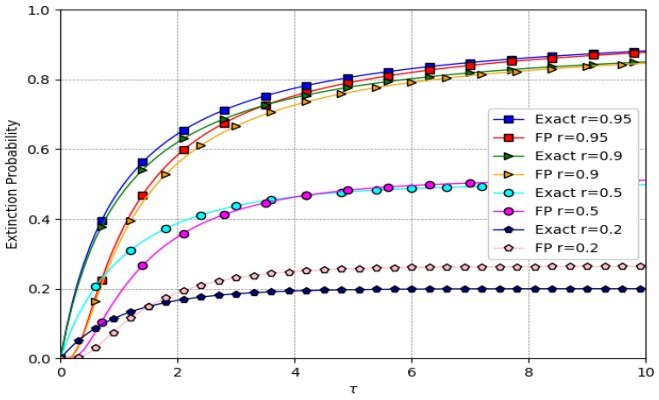

Figure 18: The extinction probability calculated by the Fokker-Plank equation compared to the exact solution for a simplified birth-death scenario for a range of r values.

With an understanding of the expected behaviour of the Itô calculus method the Pál-Bell, FPB, AMC method, and EEM method were compared against the exact solution. Figure 19 illustrates two different r values. As expected the AMC, Pál-Bell, and FPB models showed good agreement while the numerical accuracy of the Itô model decreased with reactivity.

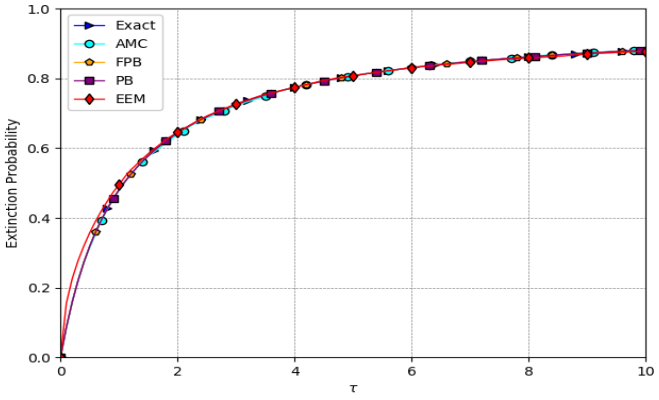

(a) $r = 0.95$

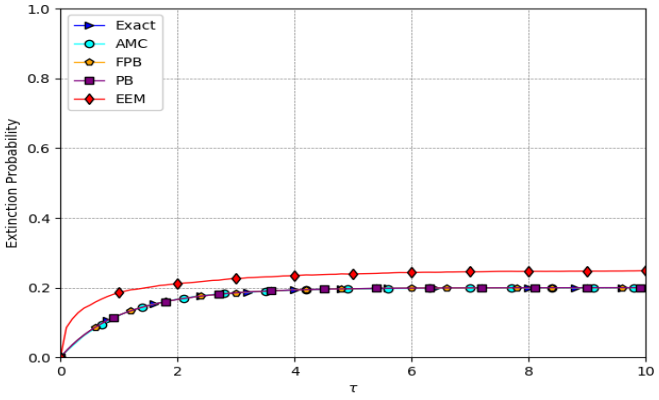

(b) $r = 0.2$

Figure 19: The extinction probability of each method compared to the exact solution for a simplified birth-death scenario.

A direct numerical comparison between the models is tabulated at $\tau = 10$ in Table 8.

Table 8: A comparison between the absolute distance of each method to the analytical solution for a simple birth-death scenario.

r	PB	FPB	AMC	EEM
0.2	6.98E-07	3.27E-07	4.64E-04	4.84E-02
0.95	1.18E-05	1.53E-05	1.08E-03	3.67E-03

Both the AMC and Itô calculus method exhibit natural variations between realisations as a result of generating random numbers in their implementation. As such, it is possible to calculate the mean and standard deviation of the binomial distribution and compare it to the results of both models:

$$\bar{x} = np \qquad \text{and} \qquad \sigma = \sqrt{np(1-p)} \tag{F.33}$$

where $\bar{x}$ is the mean, σ is the standard deviation, n is the number of realisations, and p is the extinction probability. Table 9 shows how the AMC method is within one standard deviation of the mean for all values of r, as expected for an exact method. The Itô calculus method is also less than one standard deviation from the mean for $r = 0.95$, however, as the reactivity increases the error increases significantly which supports the analysis above and offers more reason to doubt the adequacy of the method.

Table 9: The number of standard deviations from the expected extinction probability for the AMC and EEM methods at 10,000 realisations.

r	AMC	EEM
0.2	0.1	12.1
0.5	0.3	1.4
0.95	0.3	1.1

Appendix G. Wiener Process Verification

The Itô calculus approaches are the only non-exact methods considered in this paper; therefore, it can be implemented correctly and produce results that differ from the exact solution. As such, without separate verification, erroneous results would be difficult to attribute to the implementation or fundamental differences in the underlying mathematics.

Two stochastic differential equations (SDEs) [41] were modelled using the explicit Euler-Maruyama method, described in section 2.5. The results were compared against the provided source codes and showed good agreement.

The first system considered was a simplified Duffing-Van der Pol Oscillator with the following mathematical formulation:

$$dX_t = Y_t\, dt, \tag{G.1}$$

$$dY_t = (X_t(\alpha - X_t^2) - Y_t)\, dt + \sigma X_t\, dW_t \tag{G.2}$$

where $(X_0, Y_0) = (-2,0)$, $dt = 10^{-3}$, $\alpha = 1$, $\sigma = 0.5$, and $t \in [0, 1000]$. 100,000 simulations were run with the mean and variance compared at different numbers of realisations. Figure 20 illustrates a realisation of the two codes. Table 10 shows how both mean and variance of the test model and source code converge as the number of realisations increases.

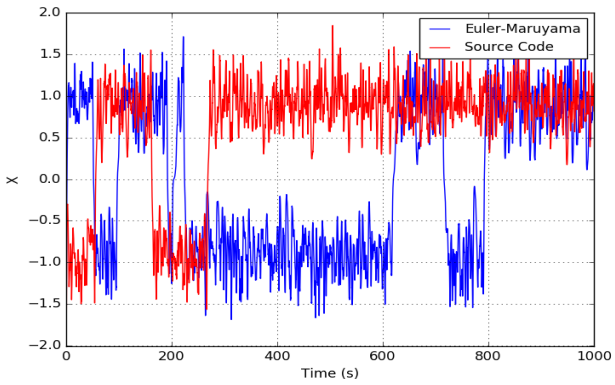

Figure 20: Duffing-Van der Pol Oscillator modelled using source code provided [41] and using the Euler-Maruyama method.

Table 10: The mean and variance of the X variable evaluated after 1,000 and 100,000 realisations.

	$\overline{X}_{1,000}$	$\overline{X}_{100,000}$	$\mu_{1,000}$	$\mu_{100,000}$
Euler-Maruyama	-0.039	0.001	0.822	0.851
Source Code	0.025	0.001	0.833	0.850

The second system considered was Geometric Brownian Motion which can be described as follows:

$$dX_t = \mu X_t\, dt + \sigma X_t\, dW_t \tag{G.3}$$

with $X_0 = 1$, $\mu = 1$, and $\sigma = 0.2$. The Euler-Maruyama was used to compute (Eq. G.3) and the results were compared to the exact solution [41]:

$$X_t = e^{\mu t} \tag{G.4}$$

Figure 21 illustrates how the mean, $\overline{X}$, converges to the exact solution as the number of realisations increases. The mean value at a time of 1 second is tabulated for different numbers of realisations in Table 11.

The results from both verification cases show good agreement and supports the implementation of the method.

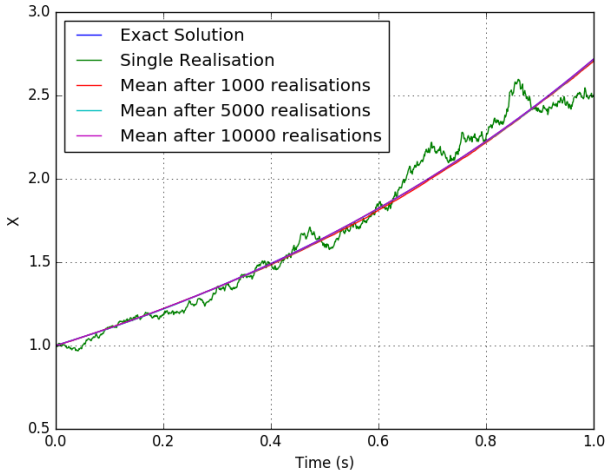

Figure 21: The Euler-Maruyama discretisaton method after an increasing number of realisations compared to the exact solution of a geometric brownian motion problem.

Table 11: The mean value computed using the Euler-Maruyama method compared to the exact solution evaluated at 1.0 second.

Exact	$\overline{\mathbf{X}}_{\mathbf{1,000}}$	$\overline{\mathbf{X}}_{\mathbf{5,000}}$	$\overline{\mathbf{X}}_{\mathbf{10,000}}$
2.718282	2.706456	2.714437	2.717588

Appendix G.1. Verification of the Itô Calculus Implementations Against Results from Literature

Three cases studies from literature [26, 28] are shown below for the verification of the explicit and implicit Euler-Maruyama implementations in this study.

Case Study 1

Table 12 shows the results of the simulation considering one group of delayed neutron precursors with the following parameters: constant reactivity $\rho(t) = -1/3$, decay constant $\lambda_1 = 0.1$ /s, delayed neutron fraction $\beta_1 = 0.05$, average neutrons per fission $\bar{\nu} = 2.5$, generation time $\Lambda = 2/3$ s, external source $q = 200$ /s, initial condition $X_0 = [400, 300]^T$, and the time domain $[0, 2]s$ with 40 time-steps. 5000 realisations were computed for each of the models to match the simulation conditions from literature.

Table 12: Verification of Euler-Maruyama implementations against Ray [26] and Suescún-Díaz [28] for Case Study 1.

	[26]	[28]	EEM	IEM
$\mathbf{E(n(2))}$	412.2	400.0	400.4	400.0
$\boldsymbol{\sigma}\mathbf{(n(2))}$	34.4	0.5	31.7	0.9
$\mathbf{E(c_1(2))}$	316.0	299.9	300.1	299.8
$\boldsymbol{\sigma}\mathbf{(c_1(2))}$	8.3	6.8	8.1	7.8

Case Study 2

Table 13 shows the results of the simulation considering six groups of delayed neutron precursors with the following parameters: constant reactivity $\rho(t) = 0.003$, decay constant $\lambda_i = [127, 317, 1150, 3110, 14000, 38700]\times10^{-4}$ /s, delayed neutron fraction $\beta_i = [266, 1491, 1316, 2849, 896, 182]10^{-6}$, average neutrons per fission $\bar{\nu} = 2.5$, generation time $\Lambda = 2\times10^{-5}$ s, external source $q = 0$ /s, initial condition $X_0 = \frac{100}{\Lambda}[1, \beta_1/\lambda_1, \beta_2/\lambda_2, ..., \beta_6/\lambda_6]^T$, and the time domain $[0, 0.1]s$ with 40 time-steps. 5000 realisations were computed for each of the models to match the simulation conditions from literature.

Table 13: Verification of Euler-Maruyama implementations against Ray [26] and Suescún-Díaz [28] for Case Study 2.

	[26]	[28]	EEM	IEM
$\mathbf{E(n(0.1))}$	208.6	179.9	175.1	180.0
$\mathbf{E(c_1(0.1))}$	4.50E+3	4.49E+3	4.49E+3	4.49E+3
$\boldsymbol{\sigma}\mathbf{(c_1(0.1))}$	1233.4	60.4	1942.0	45.8

Case Study 3

Table 14 shows the results of the simulation considering six groups of delayed neutron precursors with the following parameters: constant reactivity $\rho(t) = 0.007$, decay constant $\lambda_i = [127, 317, 1150, 3110, 14000, 38700]\times10^{-4}$ /s, delayed neutron fraction $\beta_i = [266, 1491, 1316, 2849, 896, 182]10^{-6}$, average neutrons per fission $\bar{\nu} = 2.5$, generation time $\Lambda = 2\times10^{-5}$ s, external source $q = 0$ /s, initial condition $X_0 = \frac{100}{\Lambda}[1, \beta_1/\lambda_1, \beta_2/\lambda_2, ..., \beta_6/\lambda_6]^T$, and the time domain $[0, 0.001]s$ with 40 time-steps. 5000 realisations were computed for each of the models to match the simulation conditions from literature.

Table 14: Verification of Euler-Maruyama implementations against Ray [26] and Suescún-Díaz [28] for Case Study 3.

	[26]	[28]	EEM	IEM
$\mathbf{E(n(0.001))}$	139.6	134.9	136.2	134.9
$\boldsymbol{\sigma}\mathbf{(n(0.001))}$	92.0	6.0	93.0	6.0
$\mathbf{E(c_1(0.001))}$	4.46E+3	4.46E+3	4.46E+3	4.46E+3
$\boldsymbol{\sigma}\mathbf{(c_1(0.001))}$	6.1	6.1	19.0	5.0

Good agreement is found between the explicit Euler-Maruyama method implemented in this study and the results from Ray [26]. Good agreement is also found between implicit Euler-Maruyama method implemented in this study and the results from Suescún-Díaz [28].

Appendix H. Itô Calculus discretization Methods for the Extinction Probability

As the Itô calculus method models the neutron population as a continuous variable, it is necessary to employ a discretization approximation when calculating the extinction probability. It was found that the significance of the discretization method used decreased as the extraneous neutron source strength was increased.

Three methods were employed:

1. Round down - a neutron population of 0.75 would be recorded as 0 and +1 would be added to the extinction probability for that realisation at that moment in time.
2. Round to the nearest integer - a neutron population of 0.55 would be recorded as 1 and +0 would be added to the extinction probability for that realisation at that moment in time.
3. Probability distribution - a neutron population of 0.55 would contribute +0.45 to the extinction probability for that realisation at that moment in time.

A sample result can be seen in Figure 22. As can be seen in Figure 22, there is a sharp decrease in the extinction probability for the first few time-steps. This can be attributed to the operation of the Itô calculus method. While the AMC method only has a probability of introducing a neutron into the system at the first time-step, the Itô calculus method will always do so. Therefore, without an approximation like one described above the extinction probability would start at one and instantly decrease to zero. It was found that the method of rounding down the neutron population best alleviated this problem.

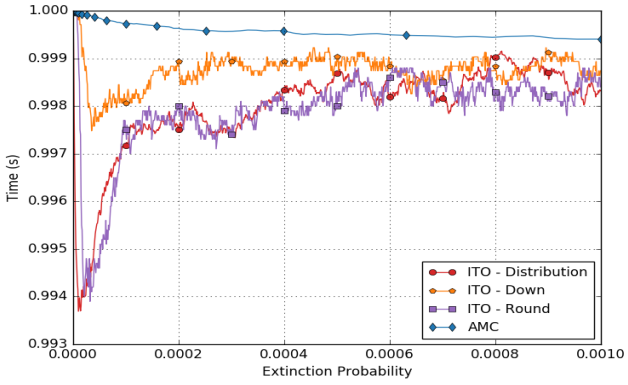

Figure 22: The different discretization methods employed in calculating the extinction probability of the Itô calculus method for a sub-critical system without delayed neutron precursors and an extraneous neutron source of 5 n/s.

Figure 23 illustrates that a realisation count of the order of 500,000 is necessary to produce a result which does not greatly fluctuate. However, Figure 23 also shows that increasing the number of realisations only increases the accuracy of the Itô calculus method in calculating the extinction probability up to a point and it does not produce a correct solution.

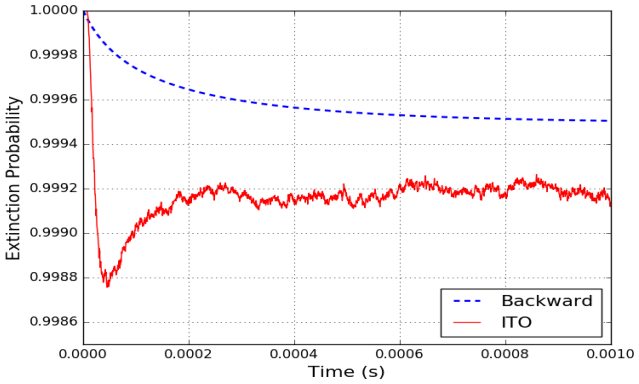

Figure 23: The extinction probability of the Pál-Bell and Itô calculus method modelling zero neutron precursor groups for the sub-critical case with an extraneous neutron source of 5 neutrons per second. 500,000 realisations were used for the Itô calculus method.

Appendix I. Itô Calculus discretization Performance

The Itô calculus method is subject to the law of diminishing returns in regards to performance. Taking the results of Pál-Bell equations to be accurate for calculating the extinction probability, the error in the Itô calculus method can be compared for different discretization refinements. Figure 24 illustrates how refining the temporal discretization generates simulation times that increase exponentially for an ever diminishing accuracy.

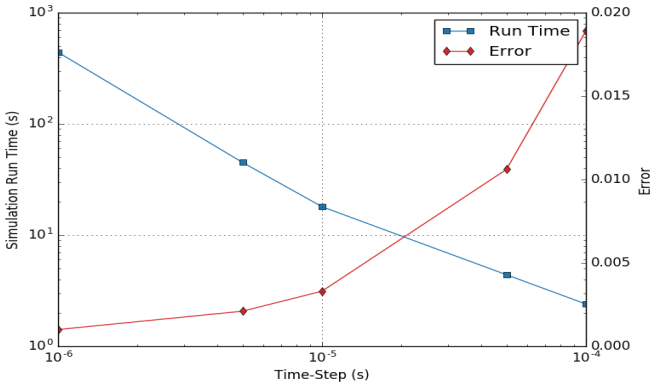

Figure 24: An example performance indicator for the Itô calculus method for a system without delayed neutron precursor groups and an extraneous neutron source of 5 n/s with $k_{\text{eff}} = 0.9$.

Appendix J. Itô Calculus Realisation Performance

The results presented in this study illustrate that the Itô calculus method utilising Euler-Maruyama discretization is unable to accurately model stochastic neutron behaviour in a variety of cases; this includes the survival and extinction probabilities, the mean and variance in very low neutron source cases, and the CDF in super-critical cases. However, Itô calculus has been shown to accurately model certain neutronic cases such as replicating experimental GODIVA results [42]. Three results from

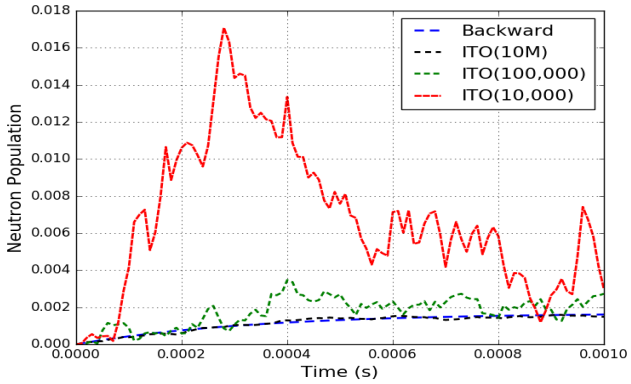

(a) 10 million realisations required for an accurate mean neutron population to be computed by the Ito-calculus approach.

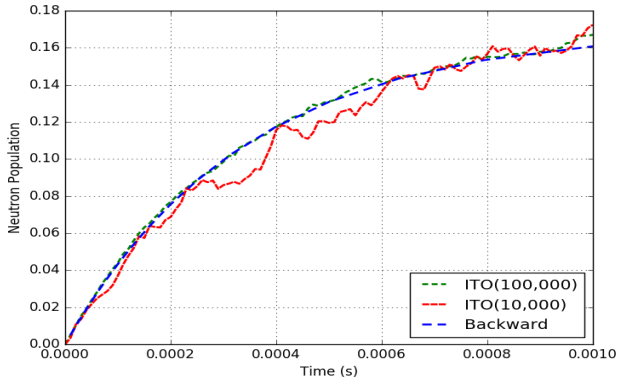

(b) 10 thousand realisations required for an accurate mean neutron population to be computed by the Ito-calculus approach.

Figure 25: The mean neutron population of the Pál-Bell and Itô calculus method modelling zero neutron precursor groups for a sub-critical case with an extraneous neutron source of 5 n/s (a) and 500 n/s (b).

the literature have also been replicated in this study [26, 28]. Therefore, the purpose of this section is to analyse the threshold neutron population above which Itô calculus is a viable method for calculating the mean neutron population.

Figure 25 shows that a large number of realisations are needed to cause the mean produced by the Itô method to be close to the correct value. More realisations are needed for a lower source strength and mean neutron population. For instance, 10 million realisations are needed for the case with a source strength of 5 n/s whilst 10,000 realisations produce a comparable agreement for the case with a source strength of 500 n/s. This means the lower the neutron population of a case, the more computational resources are required to provide a useful result.

References

[1] C. M. Cooling, M. M. R. Williams, and M. D. Eaton. Coupled probabilistic and point kinetics modelling of fast pulses in nuclear systems. *Annals of Nuclear Energy*, 94:655–671, 2016.

[2] I. Pázsit and L. Pál. *Neutron Fluctuations*. Elsevier Science, 2007.

[3] T. Misawa, H. Unesaki, and C. Pyeon. *Nuclear Reactor Physics Experiments*. Kyoto University Press, 2010.

[4] Y. Ben-Haim. *The Assay of Spatially Random Material*. D. Reidel Publishing Company, 1985.

[5] J. E. M. Saxby, A. Prinja, and M. D. Eaton. Diffusion theory model of the neutron number probability distribution in a subcritical multiplying assembly. *Annals of Nuclear Energy*, 109:507–528, 2017.

[6] J. E. M. Saxby, A. K. Prinja, and M. D. Eaton. Energy Dependent Transport Model of the Neutron Number Probability Distribution in a Subcritical Multiplying Assembly. *Nuclear Science and Engineering*, 189:1–25, 2018.

[7] E. C. Morse. *Analytical Methods for Nonproliferation*. Springer International Publishing, 2016.

[8] I. Jovanovic and A. S. Erickson, editors. *Active Interrogation in Nuclear Security*. Springer International Publishing, 2018.

[9] G. E. Hansen. Assembly of Fission Material in the Presence of a Weak Neutron Source. *Nuclear Science and Engineering*, 8:709–719, 1960.

[10] E. F. Shores. Data updates for SOURCES-4A computer code. *Nuclear Instruments and Methods in Physics Research B*, 179:78–82, 2001.

[11] M. M. R. Williams and M. D. Eaton. A theory of low source start-up based on the Pál-Bell equations. *Annals of Nuclear Energy*, 102:317–348, 2017.

[12] M. M. R. Williams and M. D. Eaton. Corrigendum to papers: 1. A theory of low source startup based on the Pal-Bell equations [ann nucl energy 102 (2017) 317]. 2. Spatial effects in low neutron source startup and associated stochastic phenomena [ann nucl energy 111 (2018) 616]. *Annals of Nuclear Energy*, 140:107061, 2020.

[13] C. M. Cooling, M. M. R. Williams, and M. D. Eaton. CALLISTO-SPK: A stochastic point kinetics code for performing low source nuclear power plant start-up and power ascension calculations. *Annals of Nuclear Energy*, 113:319–331, 2018.

[14] D.B. MacMillan. Probability Distribution of Neutron Populations in a Multiplying Assembly. *Nuclear Science and Engineering*, 39:329–336, 1970.

[15] H. Hurwitz Jr. Approximate Analysis of Reactor Start-up Incidents. *Nuclear Science and Engineering*, 6:11–17, 1959.

[16] G. I. Bell. Probability distribution of neutrons and precursors in a multiplying assembly. *Annals of Physics*, 21:243–283, 1963.

[17] G. I. Bell, W. A. Anderson, and D. Galbraith. Probability Distribution of Neutrons and Precursors in Multiplying Medium, ll. *Nuclear Science and Engineering*, 16:118–123, 1963.

[18] T. M. Sutton, A. D. LaCharite, and A. K. Prinja. Marduk: A Monte Carlo code for analyzing stochastic neutron populations dynamics. In *International Conference on Mathematics & Computational Methods Applied to Nuclear Science & Engineering*, Jeju, Korea, April 2017.

[19] T. E. Booth. Comments on Monte Carlo Probability of Initiation Estimates for Neutron Fission Chains. *Nuclear Science and Engineering*, 166:175–178, 2010.

[20] X. Gang. The Simulation of Probability Distribution of the Burst Waiting Time of Neutron Initiation. *Nuclear Science and Engineering*, 169:56–67, 2011.

[21] L. Pál. *Statistical Theory of the Chain Reaction in Nuclear Reactors I*. Central Scientific Research Institutue for Physics of the Hungarian Academy of Science, 1961.

[22] L. Pál. *Statistical Theory of the Chain Reaction in Nuclear Reactors II*. Central Scientific Research Institutue for Physics of the Hungarian Academy of Science, 1961.

[23] L Pál. *Statistical Theory of the Chain Reaction in Nuclear Reactors III*. Central Scientific Research Institutue for Physics of the Hungarian Academy of Science, 1961.

[24] S. Saha Ray. *Fractional Calculus with Applications for Nuclear Reactor Dynamics*. CRC Press, 2016.

[25] A. A. Nahla. Analytical solution of the fractional point kinetic equation with multi-group of delayed neutrons during start-up of a nuclear reactor. *Annals of Nuclear Energy*, 99:247–252, 2017.

[26] S. Saha Ray and A. Patra. Numerical solution of fractional stochastic

neutron point kinetic equation for nuclear reactor dynamics. *Annals of Nuclear Energy*, 54:154–161, 2013.

[27] M.-A. Polo-Labarrios and G. Espinosa-Paredes. Application of the fractional neutron point kinetic equation: start-up of a nuclear reactor. *Annals of Nuclear Energy*, 46:37–42, 2012.

[28] D. Suescun-Diaz, Y. M. Oviedo-Toress, and L. E. Giron-Cruz. Solution of the stochastic point kinetics equations using the implicit Euler-Maruyama method. *Annals of Nuclear Energy*, 117:45–52, 2018.

[29] M. M. R. Williams and L. Pázsit. The time dependence of the extinction probability with delayed neutrons. *Annals of Nuclear Energy*, 75:107–115, 2015.

[30] M. M. R. Williams. *Random Processes in Nuclear Reactors*. Pergamon Press, 1974.

[31] G. E. Winter, C. M. Cooling, M. M. R. Williams, and M. D. Eaton. Importance of parametric uncertainty in predicting probability distributions for burst wait-times in fissile systems. *Annals of Nuclear Energy*, 119:117–128, 2018.

[32] J. E. M. Saxby, M. M. R. Williams, and M. D. Eaton. The energy dependent Pál-Bell equation and the influence of the neutron energy on the survival probability in a supercritical medium. *Annals of Nuclear Energy*, 92:413–418, 2016.

[33] M. M. R. Williams and M. D. Eaton. Spatial effects in low neutron source start-up and associated stochastic phenomena. *Annals of Nuclear Energy*, 111:616–634, 2018.

[34] M. M. R. Williams. Approximate Methods for Inverting Generating Functions from the Pál-Bell Equations for Low Source Problems. *Nuclear Science and Engineering*, 193:327–345, 2019.

[35] M. M. R. Williams. ADDENDUM: Approximate Methods for Inverting Generating Functions from the Pál-Bell Equations for Low Source Problems. *Nuclear Science and Engineering*, 194:84–85, 2020.

[36] H. Hurwitz Jr, D. B Macmillan, J. H. Smith, and M. L. Storm. Kinetics of Low Source Reactor Startups. Part II. *Nuclear Science and Engineering*, 15:187–196, 1963.

[37] W. M. Stacey. *Nuclear Reactor Physics*. Wiley-VCH, second edition, 2007.

[38] D. R. Harris. *Naval Reactors Physics Handbook Vol I, Selected Basic Techniques, A. Radkowsky, Ed*. United States Atomic Energy Commission, 1964.

[39] E. J. Allen. *Modelling with Itó Stochastic Differential Equations*. Springer, 2007.

[40] A. Dalfes. THE FOKKER-PLANCK AND LANGEVIN EQUATIONS OF A NUCLEAR REACTOR. *Nukleonik*, 5:348–352, 1963.

[41] D. P. Kroese, T. Taimre, and Z. I. Botev. *Handbook of Monte Carlo Methods*. John Wiley & Sons, Ltd, 2011.

[42] J. G. Hayes and E. J. Allen. Stochastic point-kinetics equations in nuclear reactor dynamics. *Annals of Nuclear Energy*, 32:572–587, 2005.